Understanding the role of designed solid acid sites in the low-temperature production of ε-caprolactam

Matthew E. Potter,[a] Stephanie Chapman,[a] Alexander J. O'Malley,[b],[c] Alan Levy,[d] Marina Carravetta,[a] Thomas M. Mezza,[e] Stewart F. Parker[f] and Robert Raja[a]*

Abstract: Modern society is placing increasing demands on commodity chemicals, driven by the ever-growing global population and the desire for improved standards of living. As the polymer industry grows, a sustainable route to ε-caprolactam, the precursor to the recyclable nylon-6 polymer, is becoming increasingly important. To this end, we have designed and characterized a recyclable SAPO catalyst using a range of characterization techniques, to achieve near quantitative yields of ε-caprolactam from cyclohexanone oxime. The catalytic process operates under significantly less energetically demanding conditions than other widely practiced industrial processes.

The nylon industry has been valued at 14 billion USD for 2019,[1,2] making the synthesis of ε-caprolactam, the precursor for recyclable nylon-6 fibers, of great relevance. The acid-catalyzed Beckmann rearrangement of cyclohexanone oxime to ε-caprolactam conventionally[3] employs aggressive reagents, thereby compromising the sustainability from an environmental and ecological perspective. This can be circumvented by a vapor-phase process with a solid-acid catalyst,[4-6] but the high temperatures required to keep both lactam and oxime in the gas-phase make this process energy intensive. A wide-range of catalysts have been investigated, however most suffer from lower selectivities and limited catalyst stability, due to the high-temperatures employed.[4-13]

The liquid-phase Beckmann rearrangement employs considerably lower temperatures than the vapor-phase process, reducing energy consumption, though typically at the cost of conversion and yields, often requiring considerable solvent quantities for product separation.[14-16] As such, we recognize the need for a heterogeneous catalyst, which comprises a targeted, active site (single-site) that possesses the desired acid-strength to deliver high catalytic activities and selectivities under benign conditions. Aluminophosphates (AlPOs) are prime candidates, as their porous architectures offer high selectivity, akin to zeolites. Moreover, incorporating small quantities of dopants into an AlPO creates Brønsted acid sites, that can vary in strength, depending on the synthesis procedure and framework topology.[17,18] A comparison of silicon-substituted AlPOs (SAPOs) and other porous structures emphasizes the need for a carefully designed catalyst (Figure 1, Table S1). SAPO-37 shows great potential under these conditions, but a more general trend between pore size and activity is observed for other SAPO materials. In contrast, mesoporous materials offer little impedance to molecular diffusion, but are far inferior in performance compared to SAPOs, due to the lack of Brønsted acidity.[19,20]

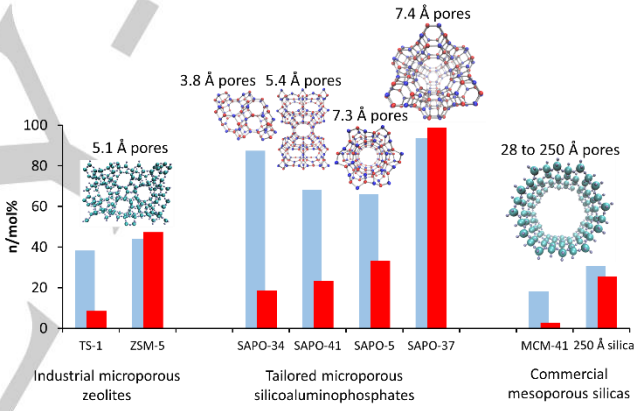

Figure 1. Contrasting the catalytic activity and selectivity of conventional microporous and mesoporous materials alongside that of the SAPOs for the liquid-phase Beckmann rearrangement of cyclohexanone oxime at 130 °C (7h) blue = caprolactam selectivity, red = conversion of cyclohexanone oxime (see also Table S1)

MAS ^{29}Si NMR was used to probe the silicon environments to elucidate the differences in catalytic behavior between the similar pore-sized (though differing framework topology) SAPO-5 and SAPO-37 catalysts. The ^{29}Si NMR spectrum of SAPO-37 shows a broad peak at -91 ppm (Figure S1), diagnostic of isomorphous substitution of Si(IV) for P(V) in the framework (note that $Si(OAl)_4$ and $Si(OAl)_3(OSi)$ are poorly-resolved due to the moisture-sensitivity of SAPO-37).[21] In contrast, SAPO-5 shows a broad peak centered at -101 ppm, indicative of silicon zoning *via* $Si(OAl)_2(OSi)_2$, $Si(OAl)(OSi)_3$, $Si(OSi)_4$ species and extra framework sites.[21,22] This produces fewer, but stronger, Brønsted acid sites on the periphery of silicon zones.[21,22] It is therefore highly likely that that the isolated acid sites observed in the SAPO-37 catalyst are more active than the acid sites associated with silicon islands.

[a] Dr. M. E. Potter, S. Chapman, Dr. M. Carravetta, Prof. R. Raja
School of Chemistry, University of Southampton, Southampton, SO17 1BJ, UK.
E-mail: R.Raja@soton.ac.uk
[b] Dr. A. J. O'Malley
UK Catalysis Hub, Research Complex at Harwell, Science and Technology Facilities Council, Rutherford Appleton Laboratory, Harwell Science and Innovation Campus, OX11 0QX, UK.
[c] Dr. A. J. O'Malley
Cardiff Catalysis Institute, School of Chemistry, Cardiff University, Cardiff, CF10 3AT, UK.
[d] Dr. A. Levy
Honeywell Int., 101 Columbia Rd, Morristown, NJ 07962, USA.
[e] Dr. T. M. Mezza
UOP LLC, 50 E. Algonquin Rd., Des Plaines, IL 60016, USA.
[f] Dr. S. F. Parker
ISIS Neutron and Muon Facility, Science and Technology Facilities Council, Rutherford Appleton Laboratory, Harwell Science and Innovation Campus, OX11 0QX, UK.

Supporting information for this article is given via a link at the end of the document.

To investigate the interactions between the SAPO-37 framework and cyclohexanone oxime, inelastic neutron scattering (INS) spectroscopy was employed. INS spectra are dominated by vibrations involving motion of hydrogen, other elements having only a minor contribution. The framework is transparent to neutrons throughout the diagnostic fingerprint region (0 – 1800 cm^{-1}), allowing the oxime and lactam to be probed as a physical mixture (10% cyclohexanone oxime and 90% SAPO-37, Figure 2). At 363 K the spectra align closely with the bulk oxime, suggesting a physical mixture of catalyst and the oxime substrate. This suggests the substrate has not properly adsorbed/entered the pores. Heating through a range of temperatures shows a progression to bands associated with the caprolactam, which is particularly noticeable at 393 K to 403 K, highlighting the significant potential of solid SAPO-37 as a low-temperature (250 ^{o}C lower than conventional methods), liquid-phase Beckmann rearrangement catalyst.

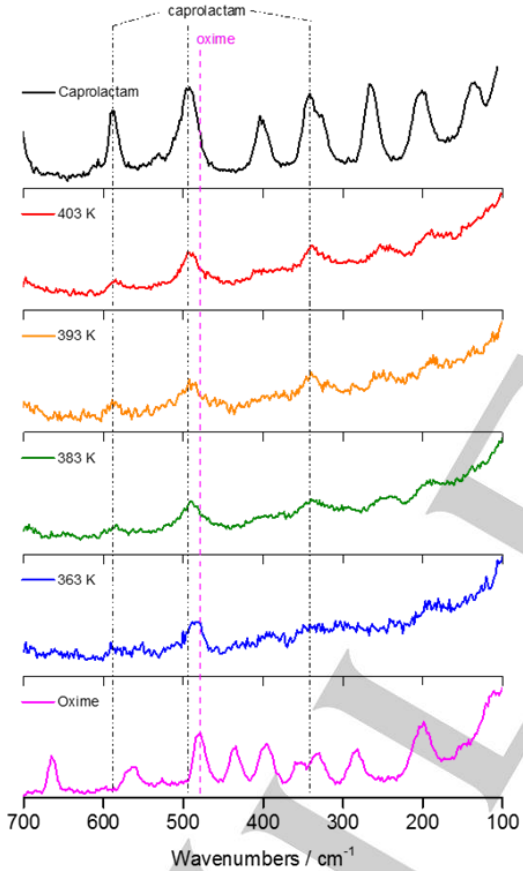

Figure 2. Variations in the INS vibrational spectrum of a cyclohexanone oxime/SAPO-37 mixture on increasing temperature.

To further optimize the SAPO-37 catalyst, a range of Si:P gel ratios were investigated (Table S2). It was revealing that minimal amounts of Si in the synthesis gel (ratio of 0.11) promotes the formation of the more thermodynamically stable AFI phase. However SAPO-37(0.21), (0.42) and (0.63) showed near-identical powder-XRD patterns, confirming their crystallinity and phase-purity (Figure S2). Moreover, unit cell parameters were found to increase with increased silicon content, indicative of isomorphous substitution of Si(IV) for P(V).[22] The textural properties of the three SAPO-37 catalysts were in agreement with each other and with literature values (Figures S3-S5).[23] 2D MAS ^{29}Si NMR showed the effect of silicon loading on the distribution of silicon environments (Figures 3A-C and S1, S6 and S7). For increased resolution, experiments were performed under a constant flow of dry nitrogen for drive, purge and bearing. As a result, individual peaks at -98 and -93 ppm were resolved and assigned as $Si(OAl)_3(OSi)$ (from 5-silicon islands) and the isolated $Si(OAl)_4$ weak Brønsted acid species, respectively. The latter typically manifests between -89 and -92 ppm, but the anhydrous nature of the experiment is believed to alter peak position slightly. The spectra show that higher silicon loadings favor Si-O-Si bonding through an increase in the -98 ppm signal ($(Si(OAl)_3(OSi))$[22] relative to the signal at -93 ppm ($Si(OAl)_4$). Evidence for silicon clustering is seen at -101, -104 and -108 ppm in the SAPO-37(0.42) and (0.63) spectra, corresponding to $Si(OSi)_2(OAl)_2$, $Si(OSi)_3(OAl)$ and $Si(OSi)_4$ species, respectively, in both the 1D and 2D NMR spectra.[21,22] These findings suggest that a lower silicon loading is necessary to promote the $Si(OAl)_4$ environment, which is crucial for creating the desired, isolated catalytically-active sites, that are fundamental for the low-temperature Beckmann rearrangement. Despite variations in the ^{29}Si NMR, both ^{27}Al and ^{31}P NMR signals were commensurate, showing predominantly $Al(OP)_4$ and $P(OAl)_4$ signals (Figures S6 and S7), thereby vindicating the overall structural integrity of the SAPO-37 catalysts.

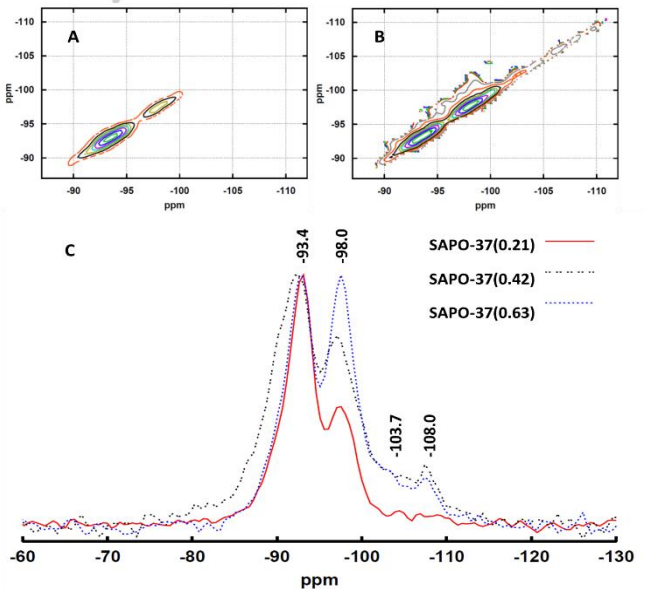

Figure 3. 2D MAS ^{29}Si NMR under N_2 of SAPO-37(0.21, (A)), SAPO-37(0.63, (B)) and 1D MAS ^{29}Si NMR of SAPO-37 containing different Si:P ratios (C).

Acid strength is also of fundamental importance in the Beckmann rearrangement.[14,16] Active sites must be sufficiently strong to form the lactam, yet weak enough to permit its subsequent desorption from the catalyst (Scheme S1).[16] Temperature programmed desorption (TPD) experiments show

that SAPO-37(0.21) and (0.42) possess a similar number of acid sites (0.93 and 0.87 mmol/g respectively), though the SAPO-37(0.63) system had fewer (0.76 mmol/g, Figures 4 and Table S3). Lower silicon loadings favor a greater number of weaker acid sites (200-400 °C), whilst increasing the silicon loading promotes the formation of stronger acid sites (400-500 °C). These observations further reinforce our earlier NMR findings.[24,25] The TPD values obtained for the SAPO-37(0.21) catalyst also correlate well with the theoretical total acidity, (Schemes S2 and S3, Table S2 and S4) calculated from the ICP and NMR data (0.98 mmol/g).

The FT-IR spectra of SAPO-37 show bands at 3641 and 3575 cm^{-1} corresponding to the hydroxyls in the supercage and sodalite cages of the faujasitic framework, respectively (Figure 4 and Figure S8). The intensity of the 3641 cm^{-1} band shows that SAPO-37(0.21) and (0.42) possess similar quantities of hydroxyl groups, in contrast to SAPO-37(0.63) (Figure S9-S11, Table S5). Low temperature CO adsorption showed only the 3641 cm^{-1} band, which was reduced significantly as a new band appeared at 3330 cm^{-1}, confirming interaction with the CO. The inflection at 3450 cm^{-1} is attributed to CO interacting with P-OH bonds, and proton migration from the sodalite cage to the supercage, making the protons accessible. The degree of the displacement of the hydroxyl band on CO adsorption is associated with the average overall acid strength of the material, which, in agreement with TPD data, increased with silicon loading (Figures S8-S11, Table S5). The CO band at 2180-2160 cm^{-1}, which can be used to quantify total acidity, highlights the similarities between SAPO-37(0.21) and (0.42), whereas SAPO-37(0.63) possesses fewer acid sites. From this data, the proton affinity was calculated as 1155, 1152 and 1146 (±5) kJ mol^{-1} for SAPO-37(0.21), (0.42) and (0.63), respectively,[26] in agreement with literature values.[27] Collidine was subsequently employed as a similar-sized probe to cyclohexanone oxime, to investigate accessibility to the active site. The bands at 1652 and 1637 cm^{-1} (O-H···N interactions, Figures S12-S15, Table S6), were quantified at different temperatures to probe acid strength. This data ratifies the observation that a lower silicon content favors more weak acid sites. Thus, by using a variety of characterization techniques, we have shown that SAPOs can be prepared with comparable physical characteristics but, by reducing silicon content, it is possible to promote the formation of isolated, weak Brønsted acid sites that are better suited for the Beckmann rearrangement. In the liquid-phase Beckmann rearrangement, variations in lactam yield and TON between the various SAPO-37 catalysts, is apparent (Table 1, S7, and Figures S16-S39). As SAPO-37(0.21) and (0.42) possess a similar quantity of acid sites, the improved selectivity for caprolactam in SAPO-37(0.21) can be attributed to the targeted weaker acid sites (Table 1). These weaker acid sites are known to enable faster lactam desorption in the vapor-phase process,[4-6] and we believe, they play a similar role in the SAPO-37(0.21) catalyst. Above 170 °C, temperature was found to have negligible effect on reaction rate, indicating that the process becomes mass-transfer limited (Table S7). Arrhenius analysis provides further confirmation that the production of caprolactam is first-order, in agreement with the mechanism postulated for the Beckmann rearrangement.[11,26,28]

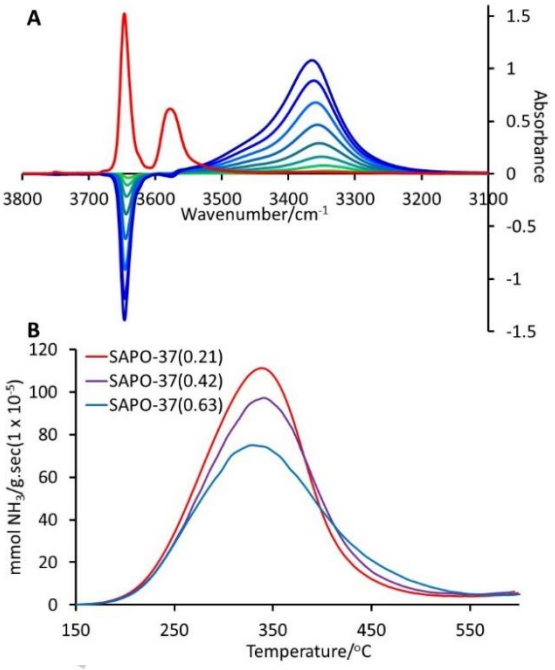

Figure 4. A) The influence of CO binding on the hydroxyl region of SAPO-37(0.21) with increasing CO_2 quantities (green to blue) while B) NH_3-TPD data reveals a greater fraction of strong acid sites with increasing Si:P ratios in SAPO-37 catalysts.

Table 1. Summary of catalytic results for the low-temperature Beckmann rearrangement of cyclohexanone oxime to ε-caprolactam (conditions as per Figure 1). [a] By-products include cyclohexanone and products from solvent-oxime reactions. [b] From NH_3-TPD. [c] From curve fitting ^{29}Si MAS NMR. [d] From collidine FT-IR.

System	Time/mins	Conversion/mol%	TON/ (mol/mol)	ε-caprolactam selectivity/mol%[a]	Total Acid quantity/(mmol/g)[b]	Degree of site isolation/%[c]	Weak + Medium acid sites/(au/mg)[d]
SAPO-37(0.21)	180	93.4	7.9	97.8	0.93	71	3.76
Anhydrous	420	99.8	8.4	97.8			
SAPO-37(0.21)	180	89.3	7.5	96.0	0.93	71	3.76
Wet	420	98.9	8.3	93.5			
SAPO-37(0.42)	180	89.8	2.9	93.3	0.87	48	3.11
Wet	420	98.8	3.2	90.3			
SAPO-37(0.63)	180	90.4	2.4	90.9	0.77	41	2.80
Wet	420	99.8	2.6	88.4			

The activation energy for SAPO-37(0.21) is lower than the SAPO-37(0.42) and (0.63) catalysts (Figure S40, Table S8) which, at 50 kJ mol^{-1}, is in good agreement with work performed in the vapor-phase,[11,28] (Scheme S4), suggesting that the reaction proceeds *via* an analogous pathway in the liquid-phase.

As water promotes site deactivation and cyclohexanone production,[16] the Beckmann rearrangement was further optimized under anhydrous conditions (Table 1, Figure S41-S44) to maximize conversion and selectivity (Table 1 and Table S9) to near-quantitative yields of ε-caprolactam. Benzonitrile is a relatively non-polar solvent and was chosen for this study, as its high boiling facilitates facile separation of caprolactam. We further confirmed the heterogeneity and stability of the SAPO-37 catalyst, which reveals sustained levels of conversion and selectivity, after several recycles (Figure S45).

In conclusion, this work represents a significant advancement in understanding how industrially attractive yields of ε-caprolactam might be achieved *via* a liquid-phase Beckmann rearrangement. We have shown how the design approach can be suitably modulated to facilitate the generation of isolated active sites, which has a direct impact on the nature and strength of the resulting solid-acid sites. Catalytic and spectroscopic protocols have been deployed to further elucidate the relationship between the nature and strength of acidic active sites and the ensuing efficiency of the SAPO-37 catalyst (Table 1) in the low-temperature Beckmann rearrangement, which affords near-quantitative yields of ε-caprolactam.

Acknowledgements

The UK Catalysis Hub is kindly thanked for resources and support provided *via* our membership of the UK Catalysis Hub Consortium. We thank the STFC Rutherford Appleton Laboratory and ISIS Pulsed Neutron and Muon Source for access to neutron beam facilities. The UK Catalysis Hub is funded by EPSRC (Engineering and Physical Sciences Research Council) *via* grants EP/K014706/1, EP/K014668/1, EP/K014854/1, EP/K014714/1 and EP/M013219/1. The EPSRC also funded the Centre for Doctoral Training scheme with grant no. EP/G036675/1. The project was also funded by the Science and Technologies Facilities Council and ISIS Pulsed Neutron Muon Source. MEP and SC also acknowledge Honeywell LLC for studentship.

Keywords: Heterogeneous catalysis • Sustainable chemistry • Beckmann rearrangement • Solid acid • Caprolactam

[1] "Nylon – A global strategic business report" Global industry analysts inc., **2010**.

[2] "World analysis – Nylon engineering resins" IHS chemicals, http://www.ihs.com/products/chemical/planning/world-petro-analysis/nylon-engineering-resins.aspx

[3] E. De Decker, J. Oostvogels, G. Van Wauwe, G. Neubauer (BASF Aktiengesellschaft) US4804754 A, **1989**.

[4] W. F. Holderich, J. Roseler, G. Heitmann, A. T. Liebens, *Catal. Today* **1997**, *37*, 353-366.

[5] G. Bellussi, C. Perego, *CATTECH* **2000**, *4*, 4-16.

[6] a) H. Ichihashi, M. Kitamura, *Catal. Today* **2002**, *73*, 23-28. b) H. Ichihasi, H. Sato, *Appl. Catal. A: Gen.* **2001**, 221, 359-366.

[7] J. Kim, W. Park, R. Ryoo, *ACS Catal.* **2011**, *1*, 337-341.

[8] H. Kath, R. Glaser, J. Weitkamp, *Chem. Eng. Technol.* **2001**, *24*, 150-153.

[9] L. Forni, G. Fornasari, C. Giordano, C. Lucarelli, A. Katovic, F. Trifiro, C. Perri, J. B. Nagy, *Phys. Chem. Chem. Phys.* **2004**, *6*, 1842-1847.

[10] E. Gianotti, M. Manzoli, M. E. Potter, V. N. Shetti, D. Sun, J. Paterson, T. M. Mezza, R. Raja, *Chem. Sci.* **2014**, *5*, 1810-1819.

[11] J. Sirijaraensre, J. Limtrakul, *ChemPhysChem* **2006**, *7*, 2424-2432.

[12] N. R. Shiju, M. Anilkumar, W. F. Holdereich, D. R. Brown, *J. Phys. Chem. C.* **2009**, *113*, 7735-7742.

[13] S. Bordiga, P. Ugliengo, A. Damin, C. Lamberti, G. Spoto, A. Zecchina, G. Spano, R. Buzzoni, L. Dalloro, F. Rivetti, *Top. Catal.* **2001**, *15*, 43-52.

[14] A. B. Fernandez, I. Lezcano-Gonzalez, M. Boronat, T. Blasco, A. Corma, *J. Catal.* **2007**, *249*, 116-119.

[15] S. Guo, Z. Du, S. Zhang, D. Li, Z. Li, Y. Deng, *Green Chem.* **2006**, *8*, 296-300.

[16] C. Ngamcharussrivichai, P. Wu, T. Tatsumi, *J. Catal.* **2005**, *235*, 139-149.

[17] J. M. Thomas, R. Raja, G. Sankar, R. G. Bell, *Nature* **1999**, *398*, 227-230.

[18] P. A. Barrett, G. Sankar, C. R. A. Catlow, J. M. Thomas, *J. Phys. Chem.* **1996**, *100*, 8977-8985.

[19] A. Jentys, N. G. Pham, H. Vinek, *J. Chem. Soc. Faraday Trans.* **1996**, *92*, 3287-3291.

[20] J. Chen, Q. Li, R. Xu, F. Xiao, *Angew. Chem. Int. Ed.* **1995**, *34*, 2694-2696.

[21] C. S. Blackwell, R. L. Patton, *J. Phys. Chem.* **1988**, *92*, 3965-3970.

[22] M. E. Potter, M. E. Cholerton, J. Kezina, R. Bounds, M. Carravetta, M. Manzoli, E. Gianotti, M. Lefenfeld, R. Raja, *ACS Catal.* **2014**, *4*, 4161-4169.

[23] H. B. Mostad, M. Stocker, A. Karlsson, T. Rorvik, *Appl. Catal. A. Gen.* **1996**, *144*, 305-317.

[24] R. Wendelbo, D. Akporiaye, A. Andersen, I. M. Dahl, H. B. Mostad, *Appl. Catal. A. Gen.* **1996**, *142*, L197-L207.

[25] G. Sastre, D. W. Lewis, C. R. A. Catlow, *J. Phys. Chem. B.* **1997**, *101*, 5249-5262.

[26] V. R. Reddy Marthala, Y. Jiang, J. Huang, W. Wang, R. Glaser, M. Hunger, *J. Am. Chem. Soc.* **2006**, *128*, 14812-14813.

[27] S. Coluccia, L. Marchese, G. Martra, *Micropor. Mesopor. Mater.* **1999**, *30*, 43-56.

[28] T. Bucko, J. Hafner, L. Benco, *J. Phys. Chem. A* **2004**, *108*, 11388-11397.

COMMUNICATION

By modulating synthesis protocols of microporous zeotypes, we optimise a heterogeneous solid acid catalyst for the low-temperature Beckmann rearrangement of cyclohexanone oxime, achieving near-quantitative yields of the Nylon-6 precursor; ε-caprolactam. Through a combination of neutron, infra-red and NMR spectroscopy we demonstrate how we determine, and target, the precise nature of the desired Bronsted acid site for selective acid catalysis.

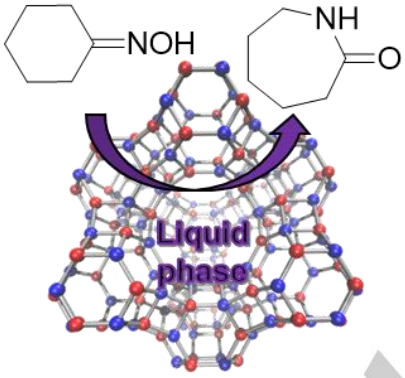

*Matthew E. Potter, Stephanie Chapman, Alexander J. O'Malley, Alan Levy, Marina Carravetta, Thomas M. Mezza, Stewart F. Parker and Robert Raja**

Page No. – Page No.

Understanding the role of designed solid acid sites in the low-temperature production of ε-caprolactam

Supporting information

Further characterisation and catalysis data **Page S3**

Contrasting zeotype frameworks for catalytic activity Page S3

^{29}Si NMR contrasting SAPO frameworks Page S3

Powder X-ray diffraction of SAPO-37 species Page S4

Scanning electron microscopy images Page S4

Further NMR spectroscopy of SAPO-37 species Page S6

Acid-site influence Page S7

Full ICP analysis Page S7

Temperature programmed desorption data Page S7

Quantitative prediction of acid sites Page S8

FT-IR data with CO probe Page S9

FT-IR data with collidine probe Page S12

Full SAPO-37 catalysis results **Page S14**

SAPO-37(0.21) Page S14

SAPO-37(0.42) Page S18

SAPO-37(0.63) Page S22

Catalysis summary Page S26

Kinetic analysis Page S27

Anhydrous catalytic data Page S28

Recycle data Page S30

Mass balance calculations Page S31

Experimental **Page S32**

Catalysis synthesis Page S32

INS measurements Page S33

ICP analysis Page S34

BET surface area measurements Page S34

Scanning electron microscopy Page S34

Powder X-ray diffraction Page S34

NMR measurements Page S34

Temperature programmed desorption Page S35

Low temperature CO adsorption FTIR Page S35

Collidine adsorption FTIR Page S35

Catalysis reactions Page S36

Kinetics and derivation Page S37

Recycles Page S38

References **Page S38**

Contrasting zeotype frameworks for catalytic activity

Table S1: Comparison of catalytic activity of different silicon-containing framework structures

System	Conversion/mol%	ε-caprolactam selectivity/mol%[a]	Pore diameter	IZA code
TS-1	8.6	38.3	5.6 Å x 5.3 Å	MFI
SAPO-5	33.2	65.9	7.3 Å x 7.3 Å	AFI
SAPO-34	18.6	87.3	3.8 Å x 3.8 Å	CHA
SAPO-37(0.21)	98.9	93.5	7.4 Å x 7.4 Å	FAU
SAPO-41	23.5	68.1	7.0 Å x 4.3 Å	AFO
SAPO-TRY	5.7	76.7	N/A	TRY

Conditions: 130 °C, Catalyst:Cyclohexanone oxime:Benzonitrile ratio 1:1:200, 0.1 g of cyclohexanone oxime, 7hrs. a) Other products include cyclohexanone and products arising from solvent-oxime interaction.

^{29}Si NMR contrasting SAPO frameworks

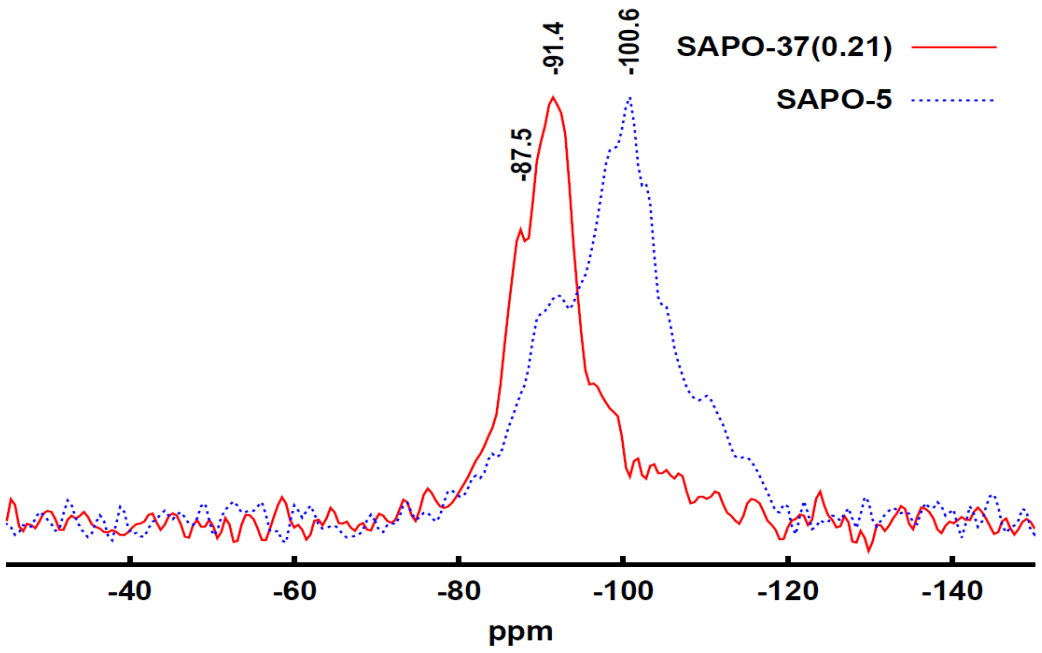

Figure S1: Comparison of SAPO-37 and SAPO-5 systems under air. This suggests silicon zoning in SAPO-5 compared to the more isomorphous Si substitution of P sites in SAPO-37 as discussed in the main article.

Powder X-ray diffraction of SAPO-37 species

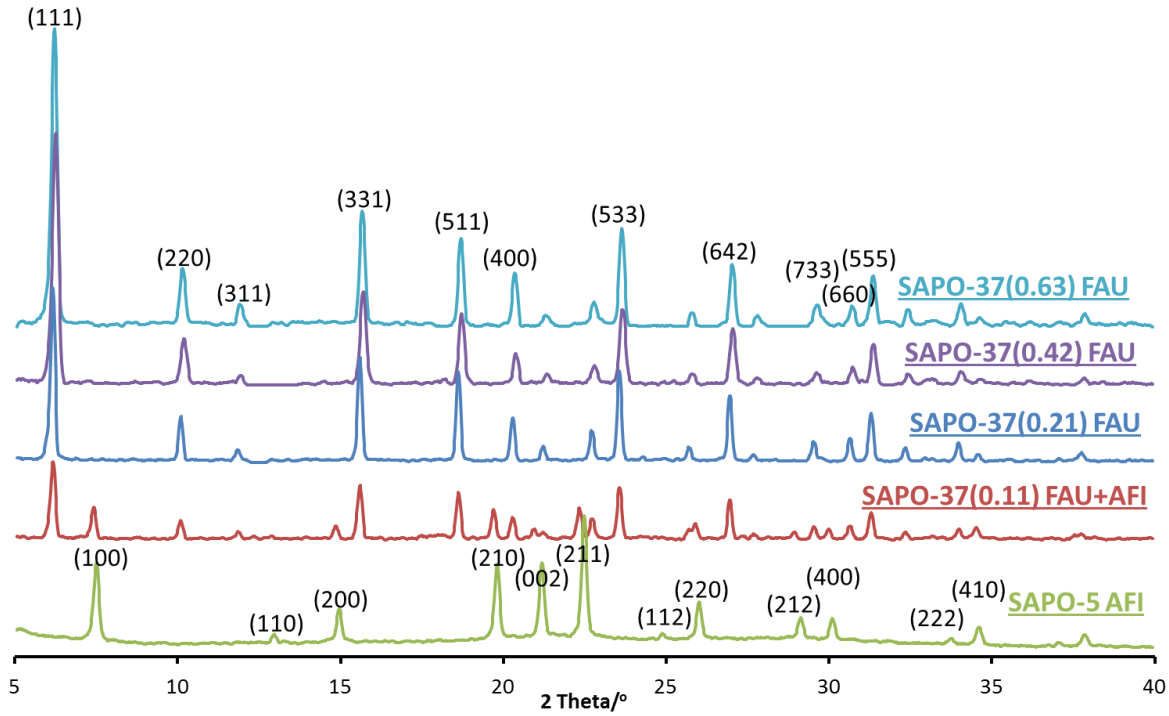

Figure S2: Comparison of powder XRD patterns confirming phase-purity at Si:P gel ratios of 0.21 and above.

Scanning electron microscopy images

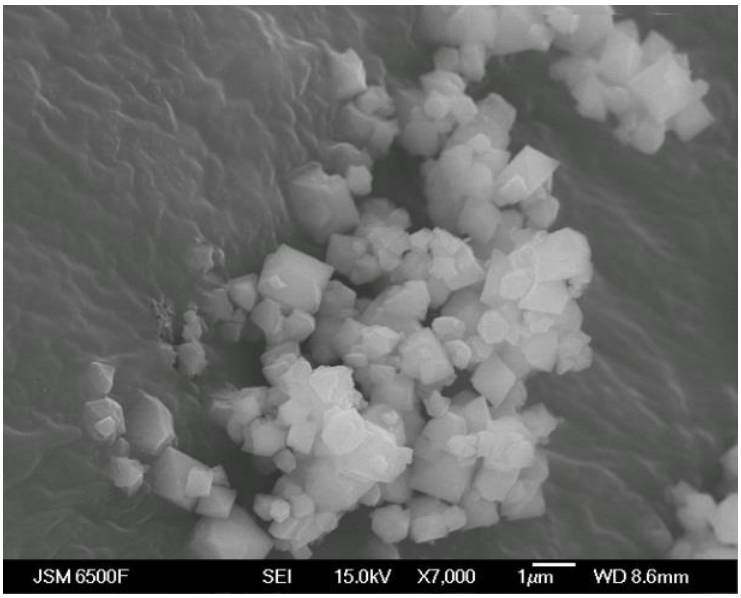

Figure S3: SEM image of SAPO-37(0.21).

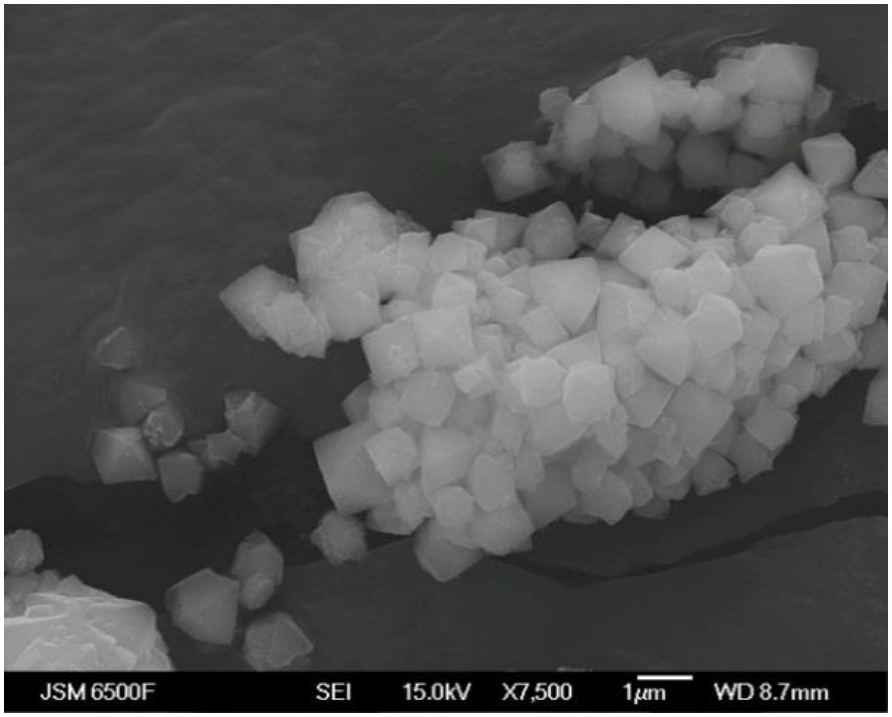

Figure S4: SEM image of SAPO-37(0.42)

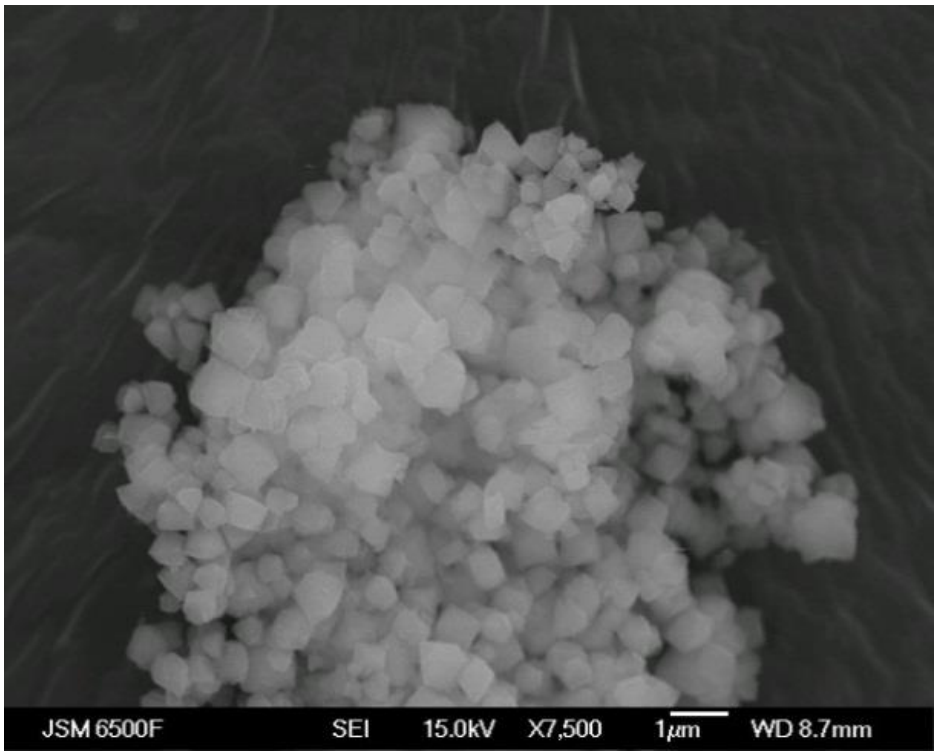

Figure S5: SEM image of SAPO-37(0.63)

Further NMR spectroscopy of SAPO-37 species

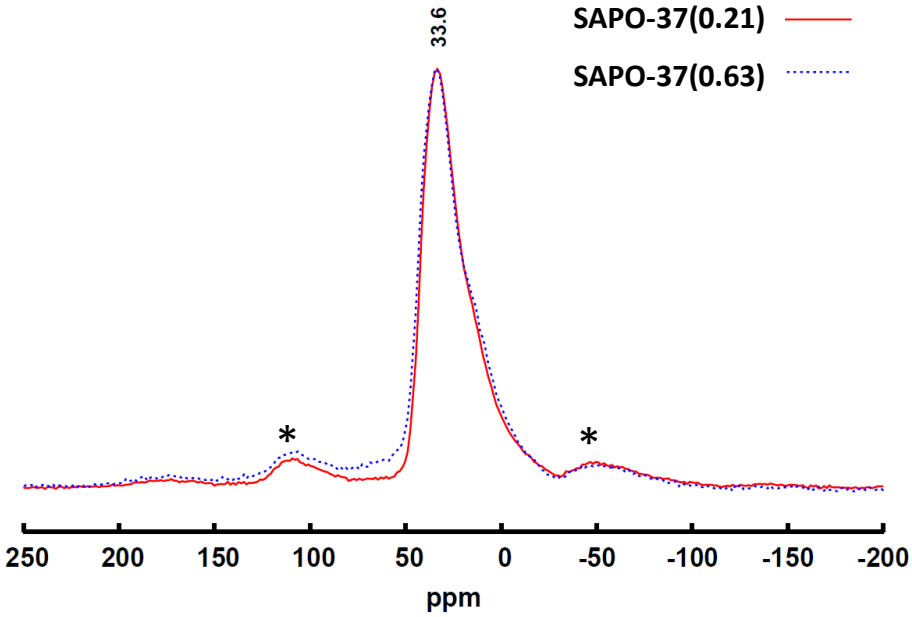

Figure S6: 1D ^{27}Al MAS NMR spectra comparing SAPO-37(0.21) and SAPO-37(0.63), *represents peaks due to spinning side-bands.

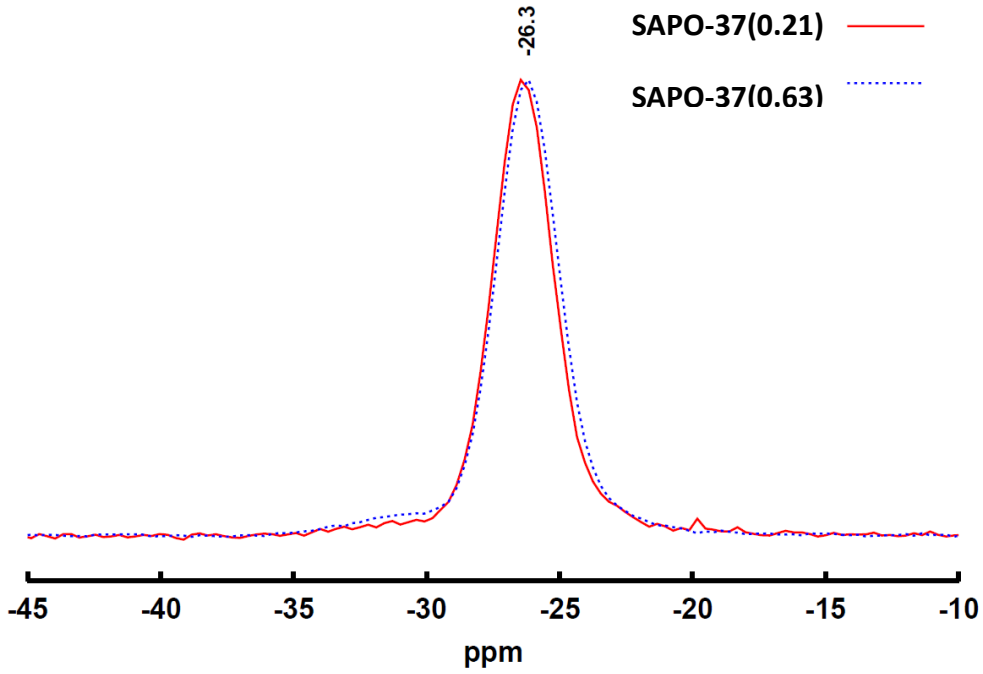

Figure S7: 1D ^{31}P MAS NMR spectra comparing SAPO-37(0.21) and SAPO-37(0.63)

Acid-site influence

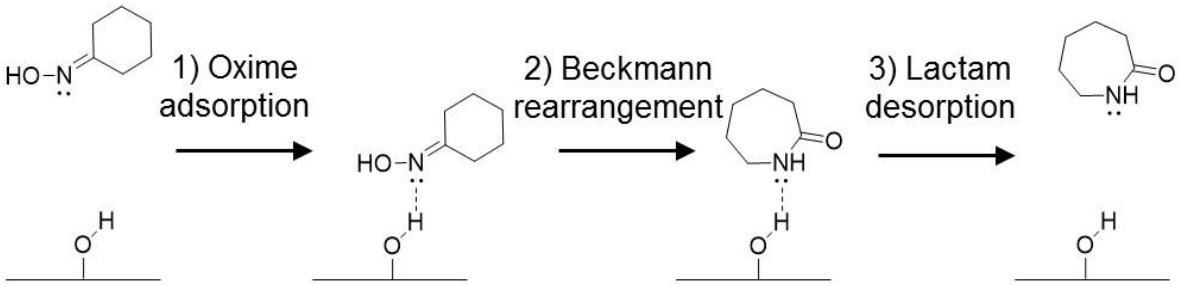

Scheme S1: Showing the steps detailing lactam formation and subsequent desorption from a solid acid catalyst.

Full ICP analysis

Table S2: Full ICP results of SAPO samples

System	Al/wt%	P/wt%	Si/wt%
SAPO-37(0.21)	23.5	20.8	2.95
SAPO-37(0.42)	20.6	19.0	7.59
SAPO-37(0.63)	21.5	16.1	9.51

Temperature programmed desorption data

Table S3: Integrated areas from NH_3-TPD.

	Integration results/(mmol/g)					
System	150 – 200 °C	200 – 300 °C	300 – 400 °C	400 – 500 °C	500 – 600 °C	Total
SAPO-37(0.21)	0.004	0.233	0.563	0.094	0.033	0.927
SAPO-37(0.42)	0.004	0.206	0.503	0.122	0.039	0.873
SAPO-37(0.63)	0.003	0.182	0.406	0.139	0.035	0.765

Quantitative prediction of acid sites

We assume that In low-silicon environments only one of two sites produce acid sites (Scheme S2 and S3). Further we assume that the peak at -93 ppm accurately quantifies the number of $Si(OAl)_4$ species, whilst the peak at -98 ppm accurately quantifies the number of $Si(OAl)_3(OSi)$ species which comes from the periphery of small silicon islands, constituting 4 $Si(OAl)_3(OSi)$ species and one $Si(OSi)_4$ species, which is attributed to the peak at -108 ppm.

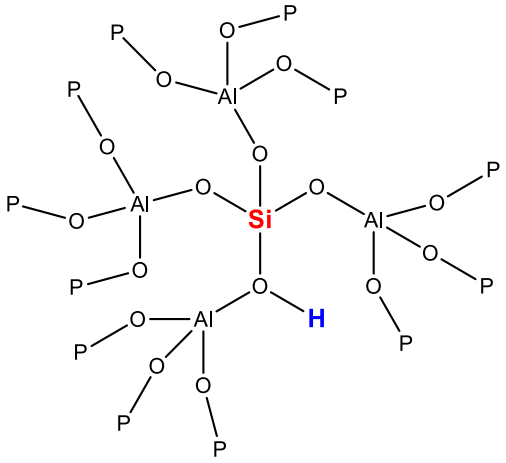

Scheme S2: Detailing the isolated acid site at -93 ppm. Red silicon atoms represent silicons incorporated through a type II mechanism, blue protons are the generated acid sites. From this we see that one silicon at -93 ppm forms one acid site.

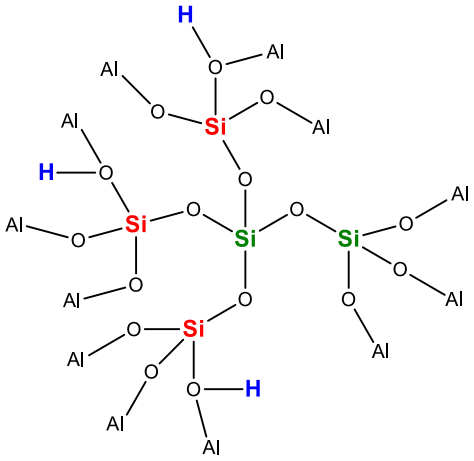

Scheme S3: Detailing the 5-silicon islands. The central silicon atom is the $Si(OSi)_4$ peak at -108 ppm. The green silicon atoms are incorporated through type III substitution, therefore do not generate a proton. The red silicon atoms are incorporated through type II substitution and generate acid sites. From this we see that five silicons form three acid sites. Therefore for every 4 silicons at -98 ppm we expect three acid sites, thus each silicon at -98 ppm is responsible for ¾ of an acid site.

The ICP shows that SAPO-37(0.21) contains 2.95 wt% of Si. The ^{29}Si NMR of SAPO-37(0.21) gives the following distribution:

Table S4: Calculation of number of acid sites in SAPO-37(0.21)

Observable peaks/ppm	Relative area	Moles of silicon per gram of SAPO-37(0.21) / mmol g^{-1}
-93	0.71	0.748
-98	0.29	0.305

From Scheme S2 and S3 we know that one mole of silicon from the peak at -93 ppm forms one acid site. One mole of silicon from the peak at -98 ppm forms 0.75 moles of an acid site.

Therefore total moles of acid is:

(0.748 x 1) + (0.305 x 0.75) = 0.977 mmol g^{-1}.

This agrees well with the NH_3-TPD value of 0.927 mmol g^{-1}

This calculation has not been attempted for the SAPO-37(0.42) and SAPO-37(0.63) as it is believed that the significant amount of clustering will mean there are a greater variety of silicon islands than those assumed, as such the calculation will be inaccurate and non-representative.

FT-IR data with CO probe

Table S5: Summary of FT-IR data on SAPO-37 samples using a CO probe

Sample	**Bridging OH band position/cm^{-1}**			**CO Area (AU) (0.18 cc add)**
	Before CO	**After CO**	**Shift**	
SAPO-37(0.21)	3646.8	3342.1	305	0.854
SAPO-37(0.42)	3646.7	3335.4	311	0.856
SAPO-37(0.63)	3646.1	3325.0	321	0.582

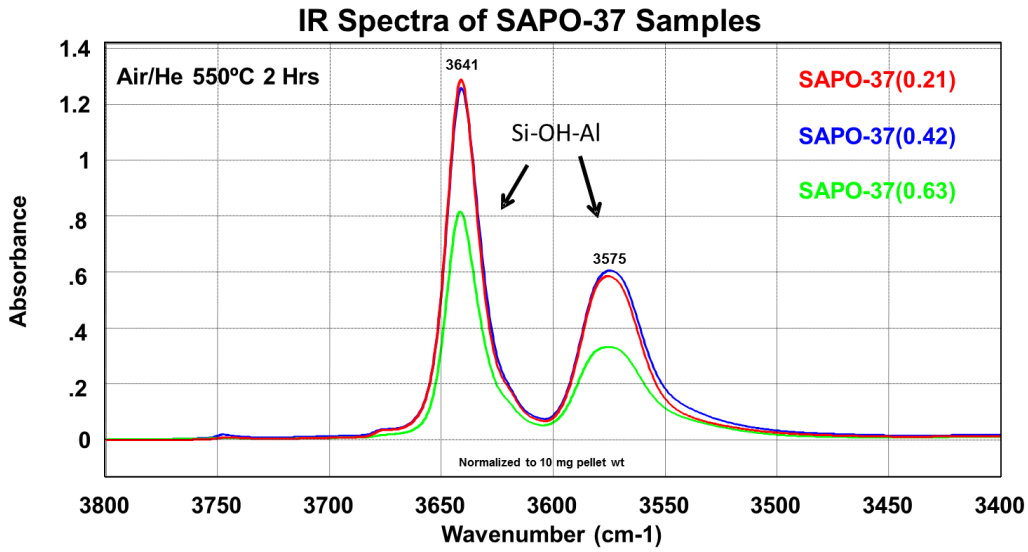

Figure S8: FT-IR spectra of the hydroxyl region of various SAPO-37 systems

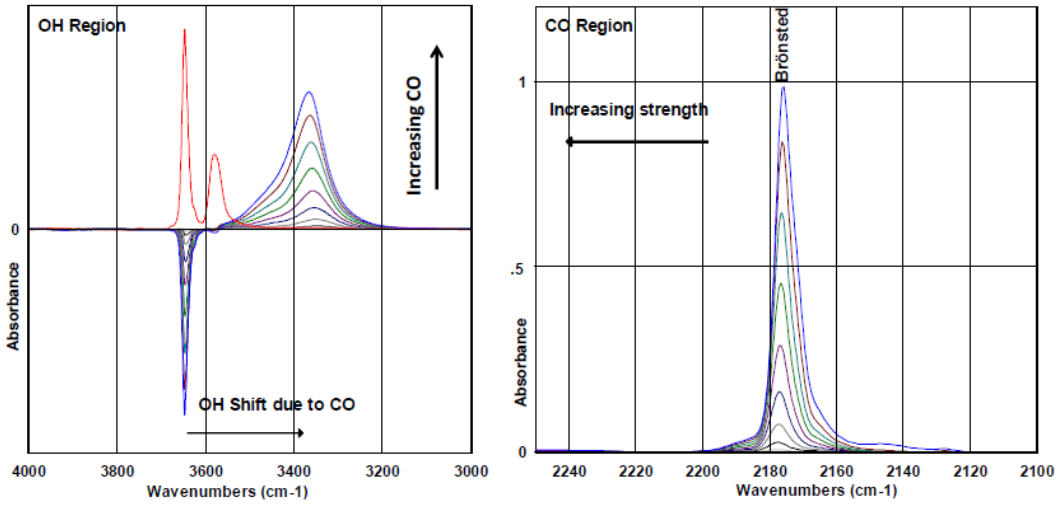

Figure S9: Difference FT-IR spectra of SAPO-37(0.21) with varying CO loadings

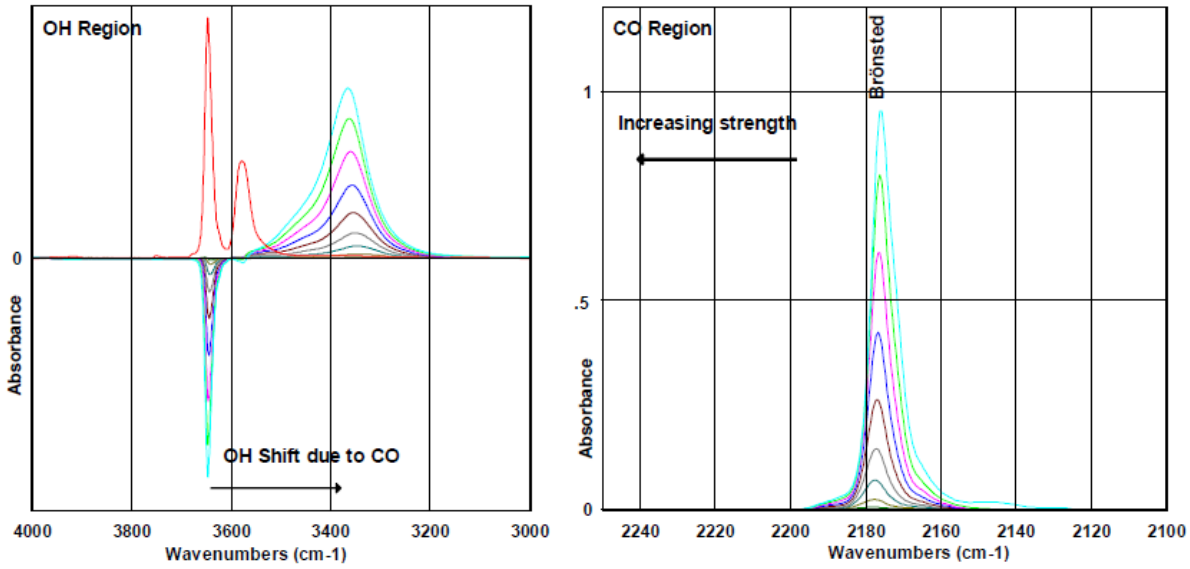

Figure S10: Difference FT-IR spectra of SAPO-37(0.42) with varying CO loadings

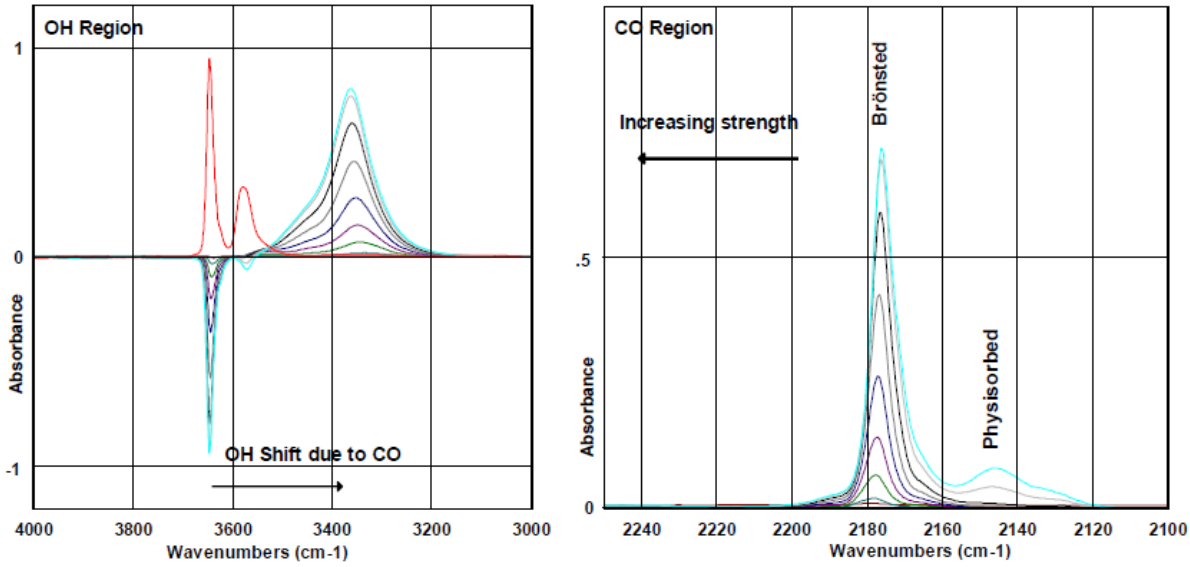

Figure S11: Difference FT-IR spectra of SAPO-37(0.63) with varying CO loadings

FT-IR data with collidine probe

Table S6: Summary of FT-IR data using collidine as a probe on SAPO-37 samples

Sample	Weak sites[a] (au/mg)	Medium sites[b] (au/mg)
SAPO-37(0.21)	0.913	2.845
SAPO-37(0.42)	0.389	2.722
SAPO-37(0.63)	0.382	2.420

a) Collidine band area after 150°C – 300°C desorption b) Collidine band area after 300°C – 450°C desorption

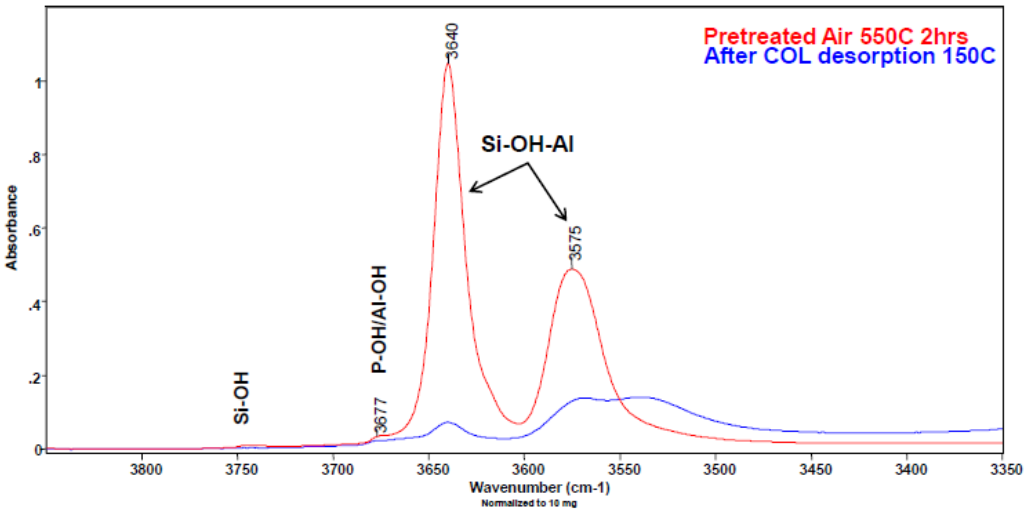

Figure S12: FT-IR spectra of SAPO-37(0.21) using collidine as a probe

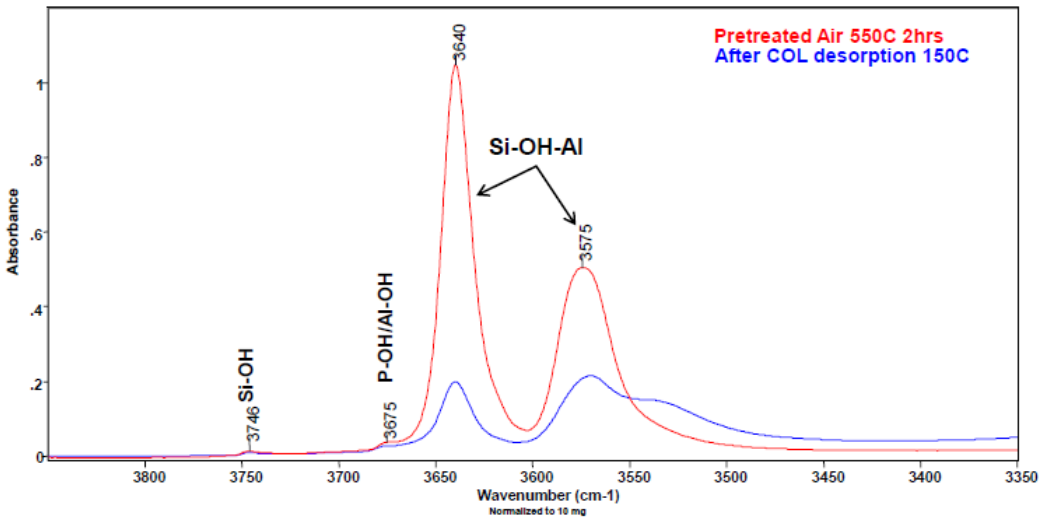

Figure S13: FT-IR spectra of SAPO-37(0.42) using collidine as a probe

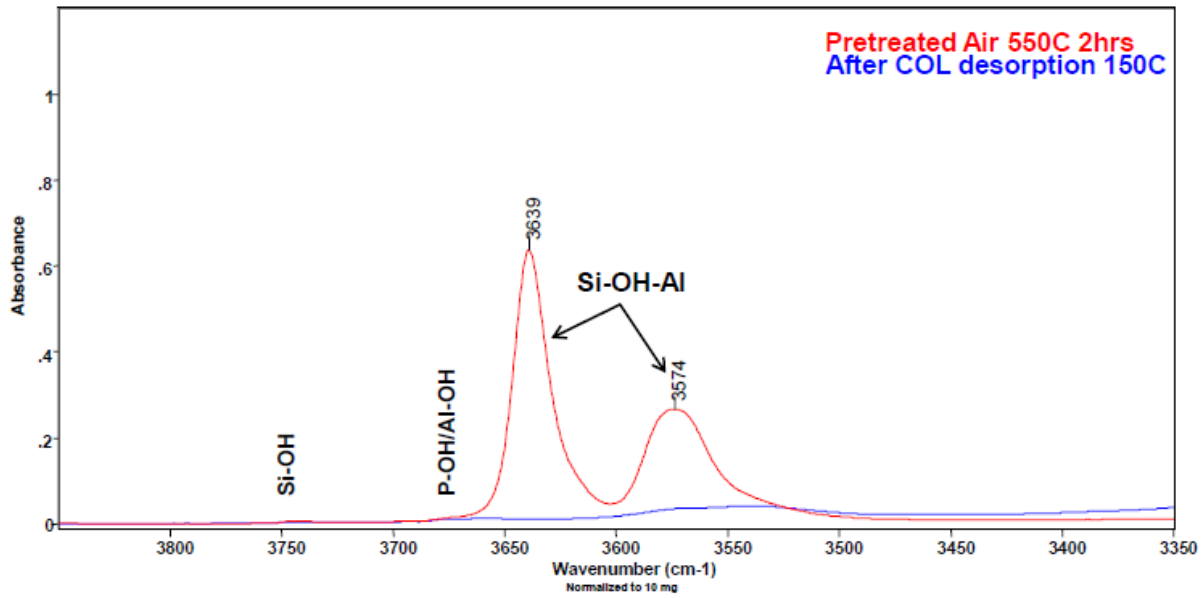

Figure S14: FT-IR spectra of SAPO-37(0.63) using collidine as a probe

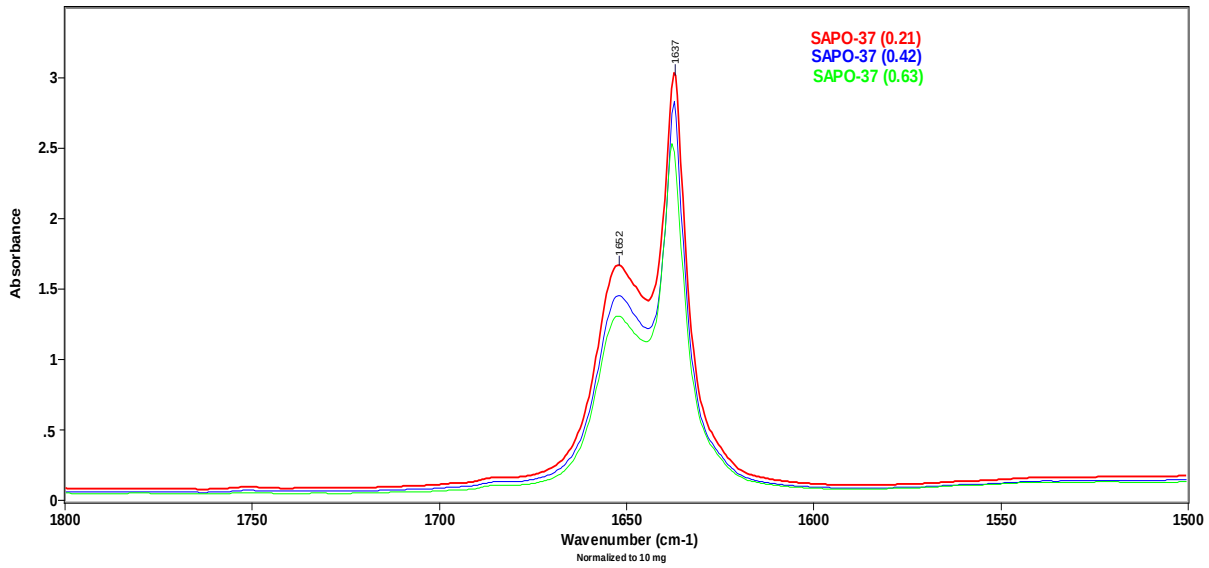

Figure S15: Difference FT-IR spectra of various SAPO-37 samples after collidine adsorption/desorption at 150°C.

Full SAPO-37 catalysis results

SAPO-37(0.21)

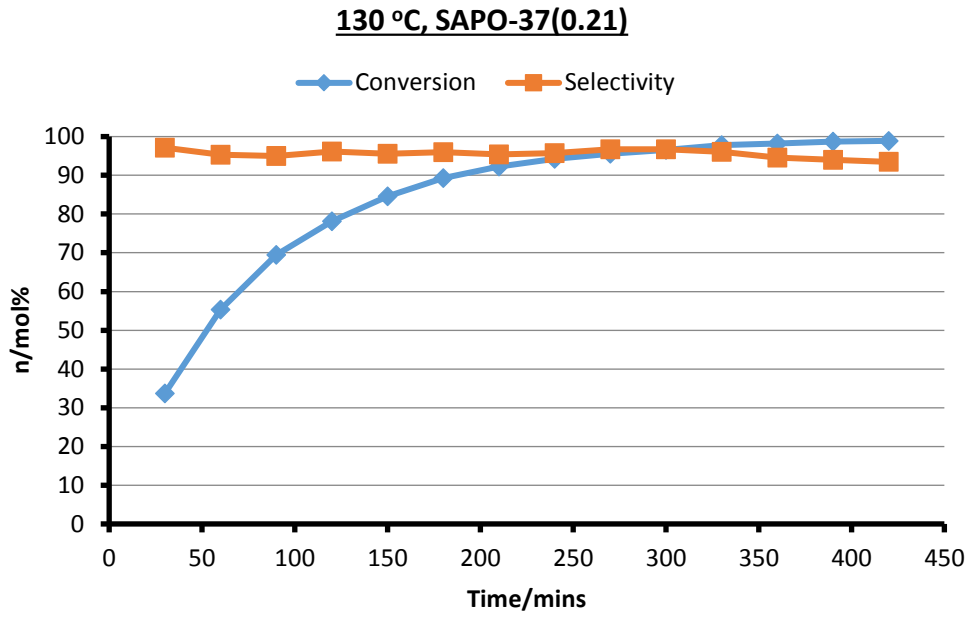

Figure S16: Catalytic data for the conversion of cyclohexanone oxime to ε-caprolactam with SAPO-37(0.21) at 130°C

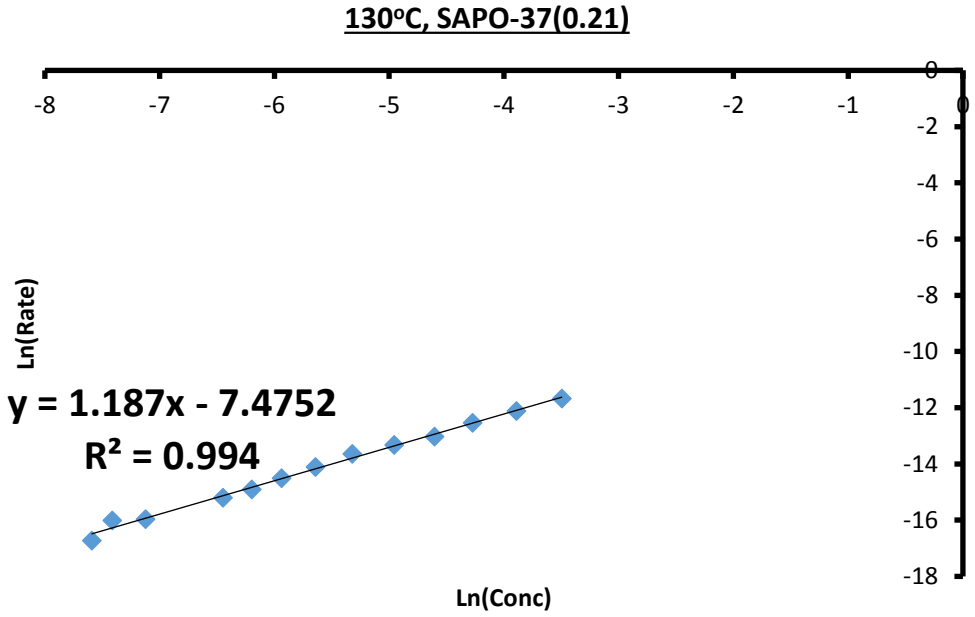

Figure S17: Graph detailing kinetic analysis of cyclohexanone oxime to ε-caprolactam with SAPO-37(0.21) at 130 °C

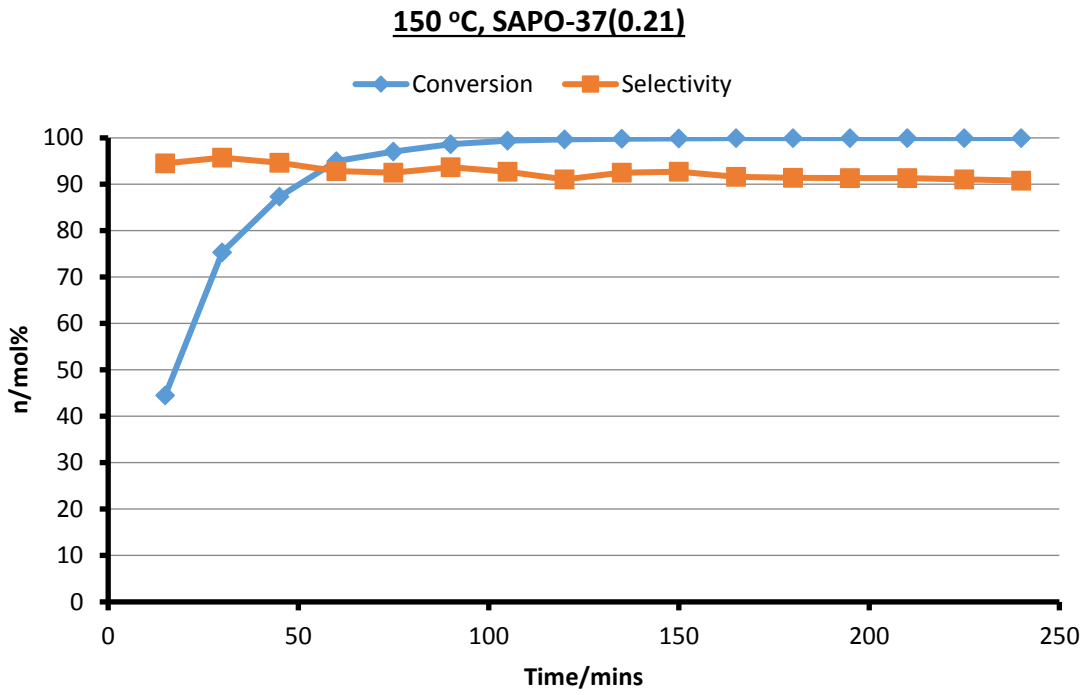

Figure S18: Catalytic data for the conversion of cyclohexanone oxime to ε-caprolactam with SAPO-37(0.21) at 150°C

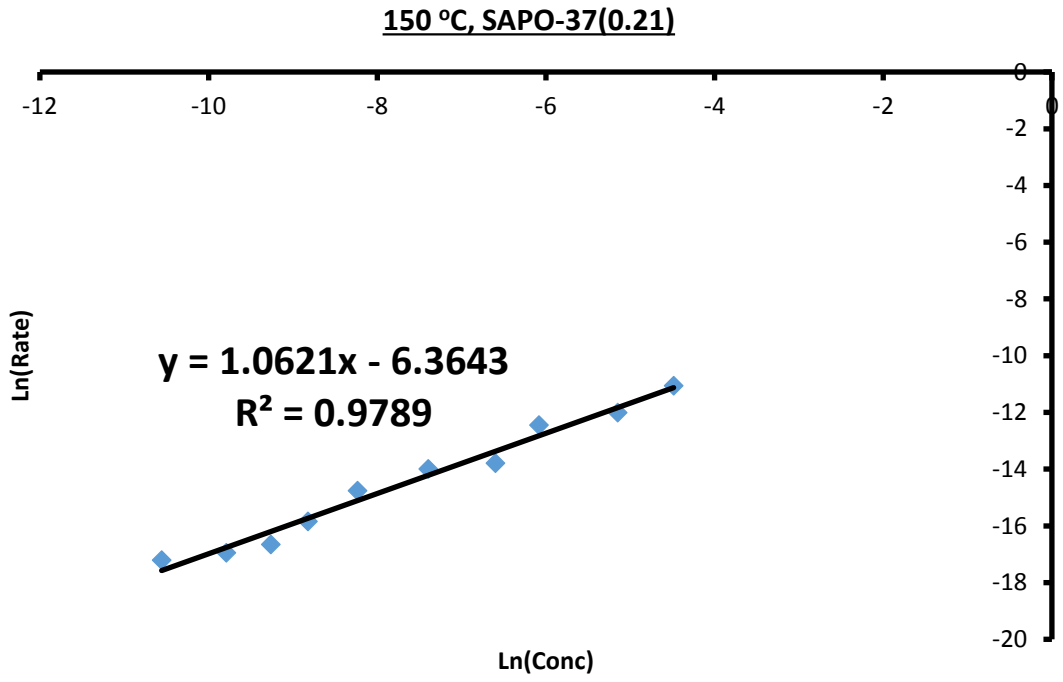

Figure S19: Graph detailing kinetic analysis of cyclohexanone oxime to ε-caprolactam with SAPO-37(0.21) at 150 °C

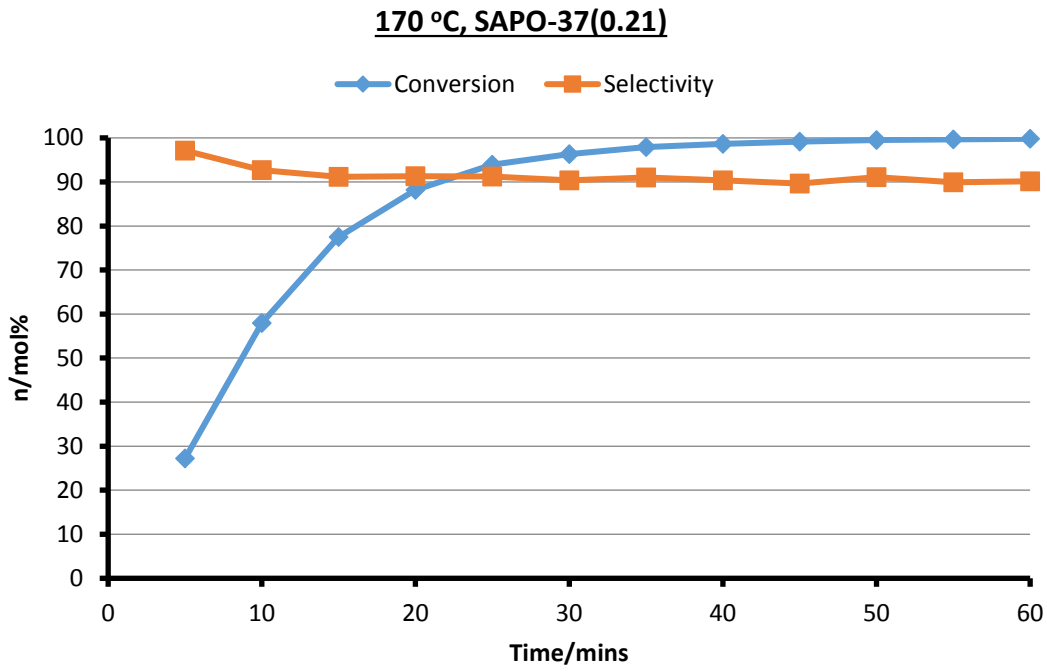

Figure S20: Catalytic data for the conversion of cyclohexanone oxime to ε-caprolactam with SAPO-37(0.21) at 170°C

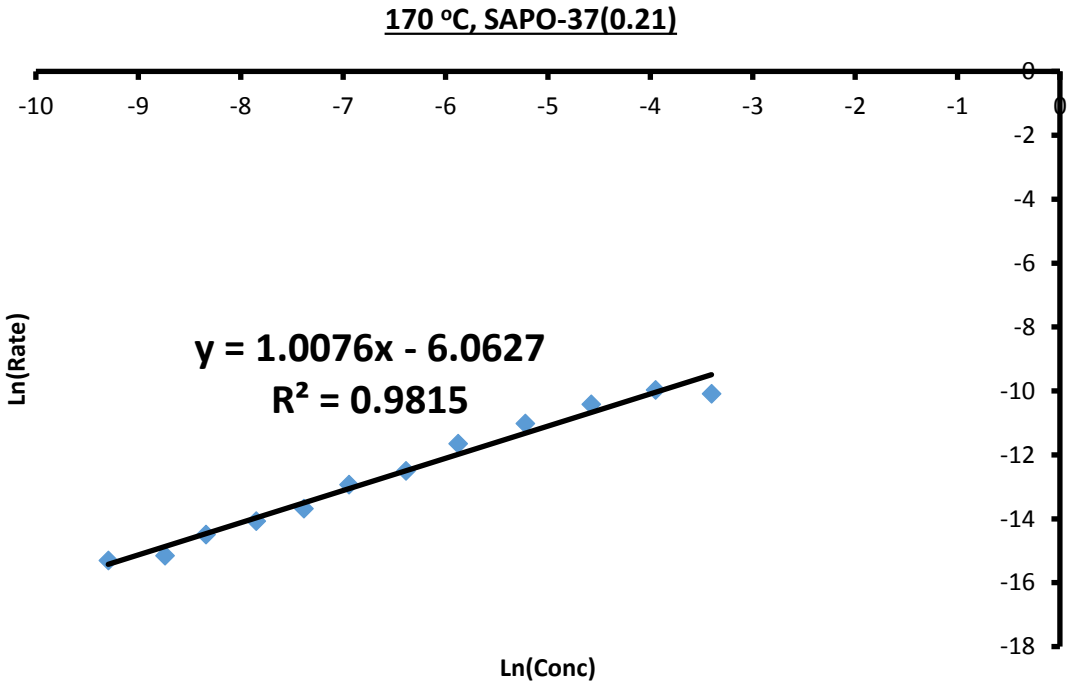

Figure S21: Graph detailing kinetic analysis of cyclohexanone oxime to ε-caprolactam with SAPO-37(0.21) at 170 °C

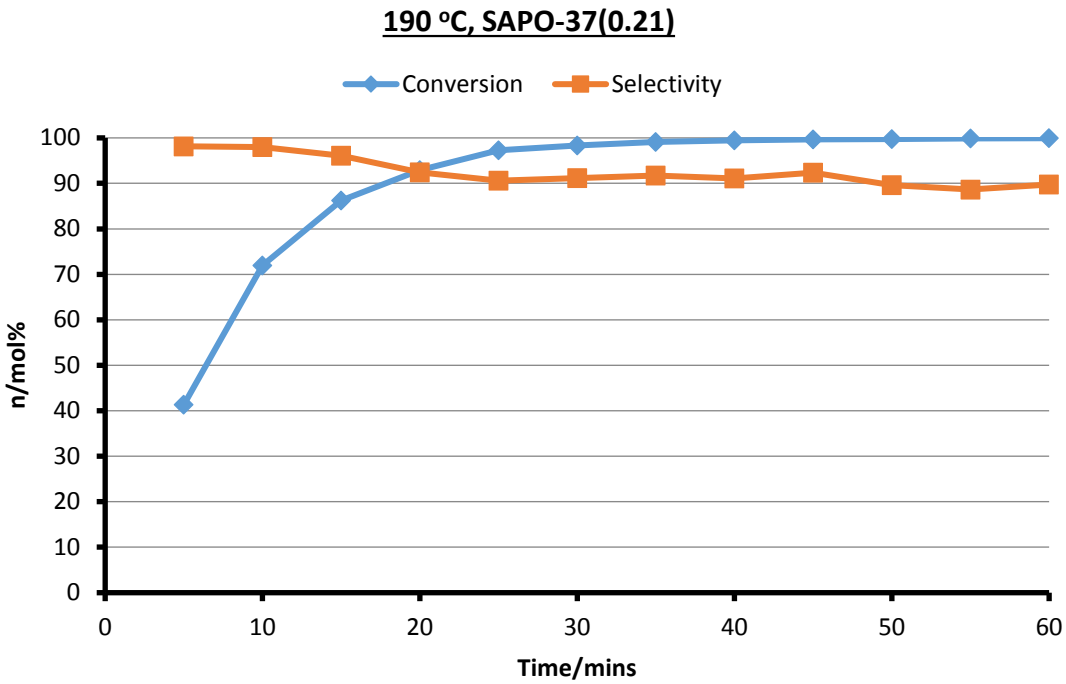

Figure S22: Catalytic data for the conversion of cyclohexanone oxime to ε-caprolactam with SAPO-37(0.21) at 190°C

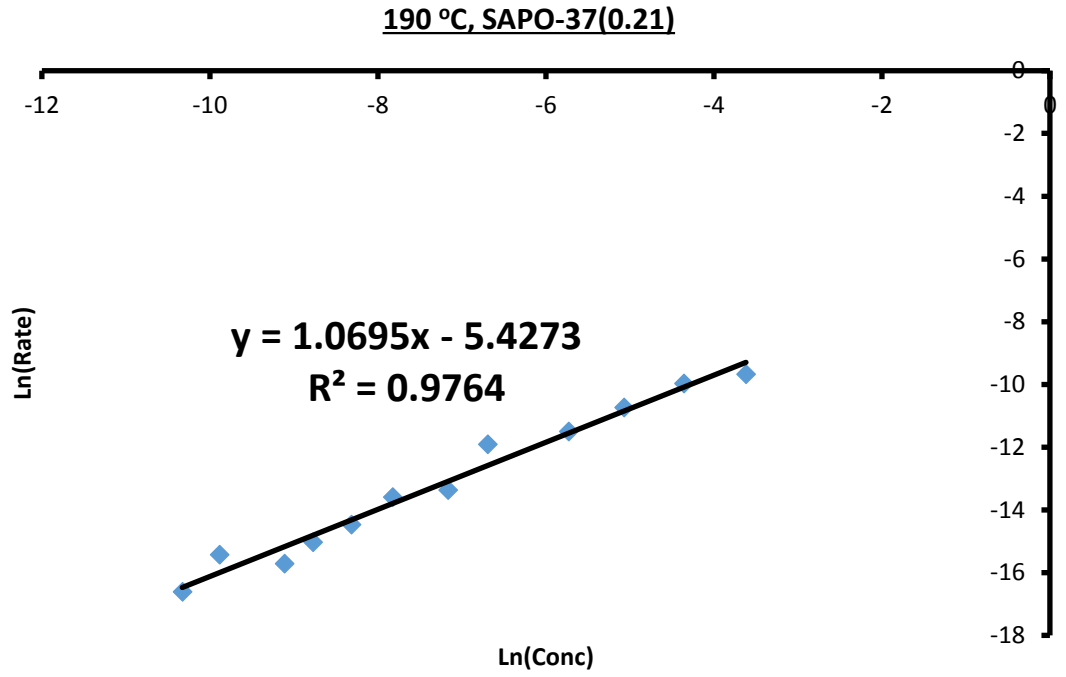

Figure S23: Graph detailing kinetic analysis of cyclohexanone oxime to ε-caprolactam with SAPO-37(0.21) at 190 °C

SAPO-37(0.42)

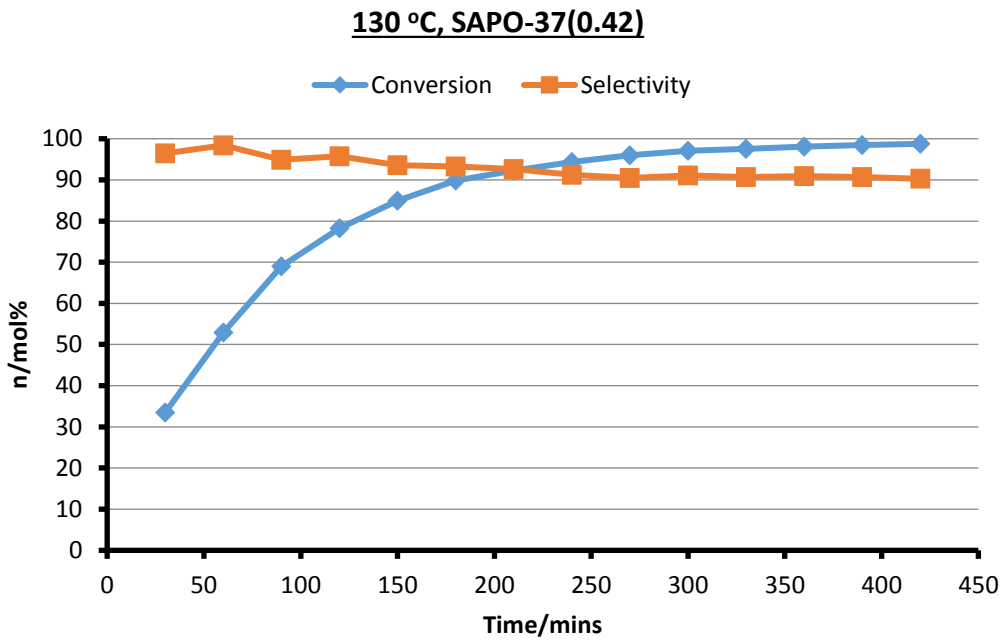

Figure S24: Catalytic data for the conversion of cyclohexanone oxime to ε-caprolactam with SAPO-37(0.42) at 130°C

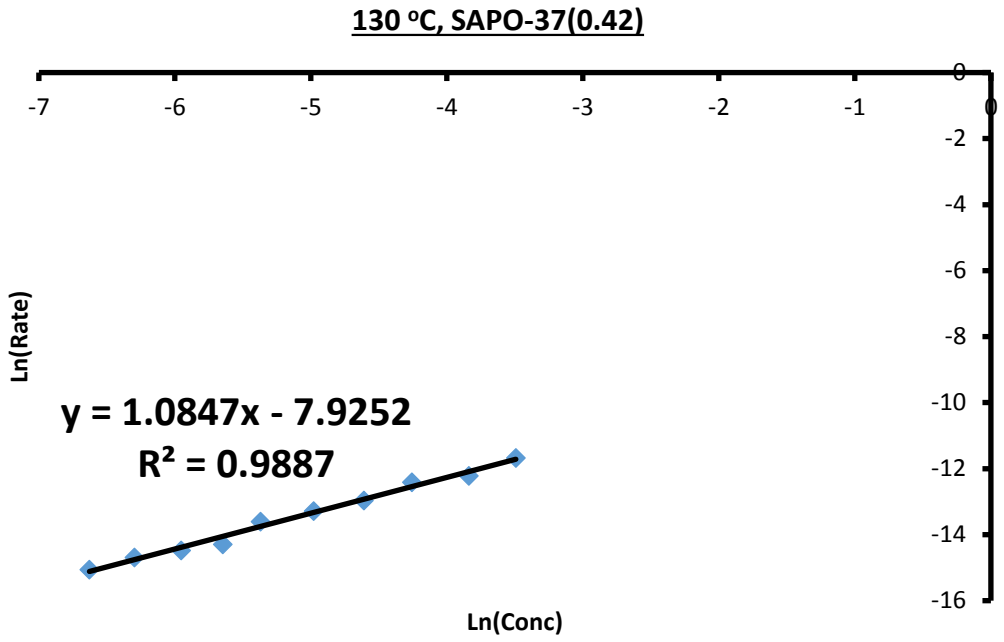

Figure S25: Graph detailing kinetic analysis of cyclohexanone oxime to ε-caprolactam with SAPO-37(0.42) at 130 °C

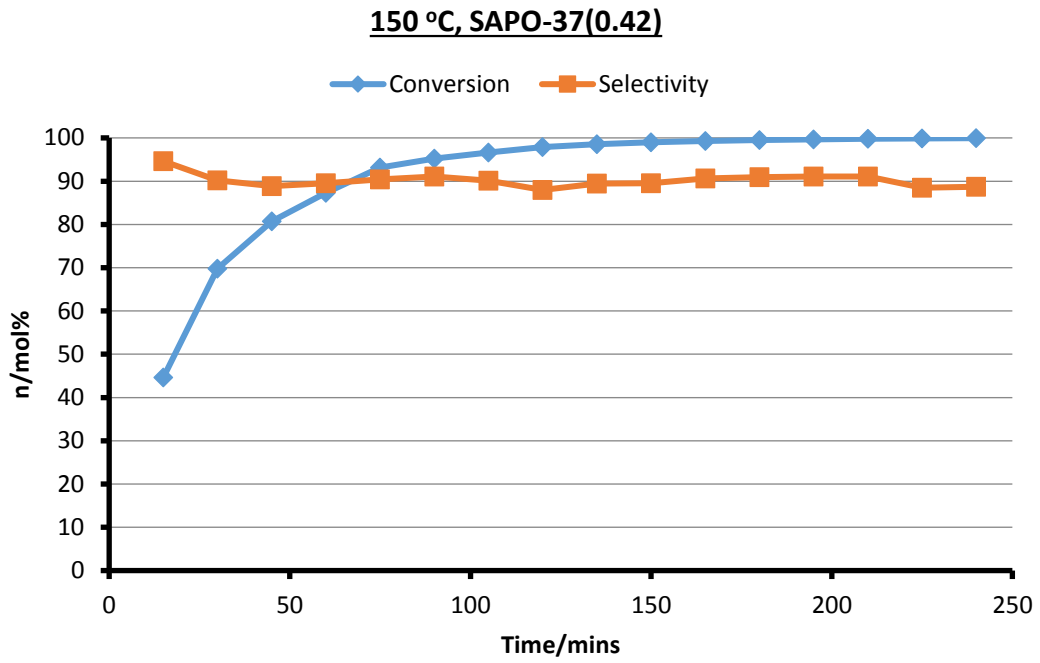

Figure S26: Catalytic data for the conversion of cyclohexanone oxime to ε-caprolactam with SAPO-37(0.42) at 150°C

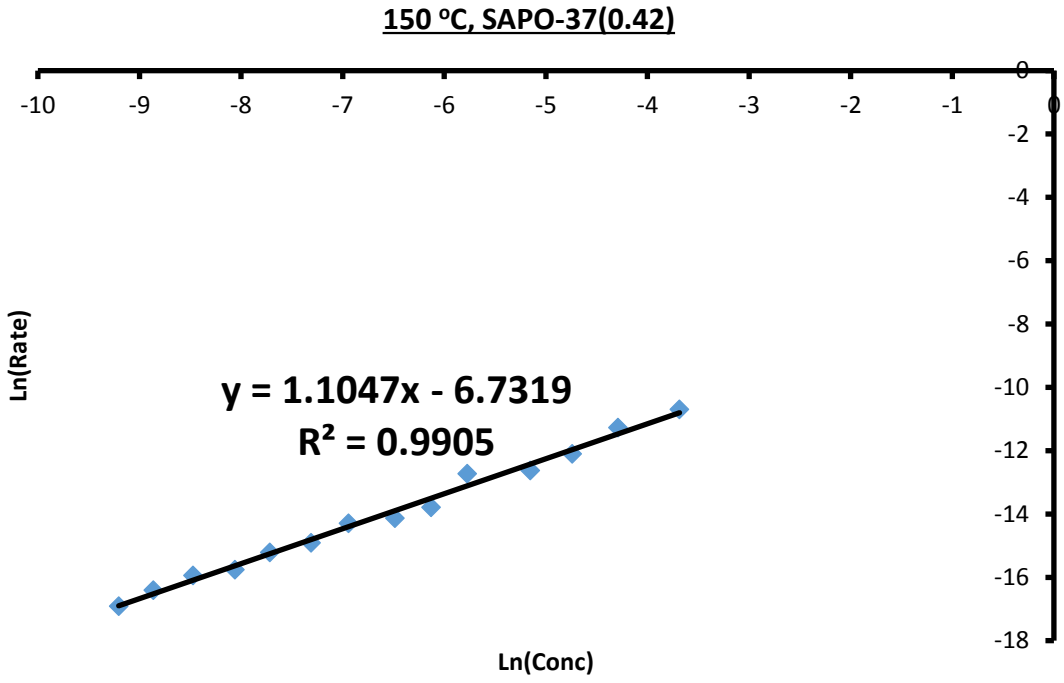

Figure S27: Graph detailing kinetic analysis of cyclohexanone oxime to ε-caprolactam with SAPO-37(0.42) at 150 °C

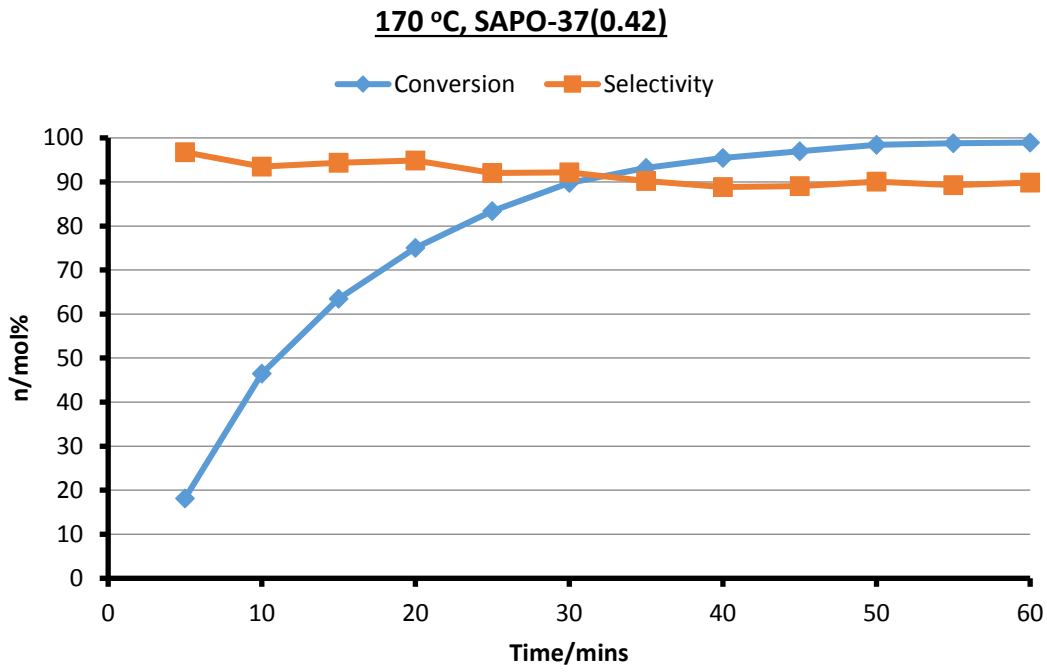

Figure S28: Catalytic data for the conversion of cyclohexanone oxime to ε-caprolactam with SAPO-37(0.42) at 170°C

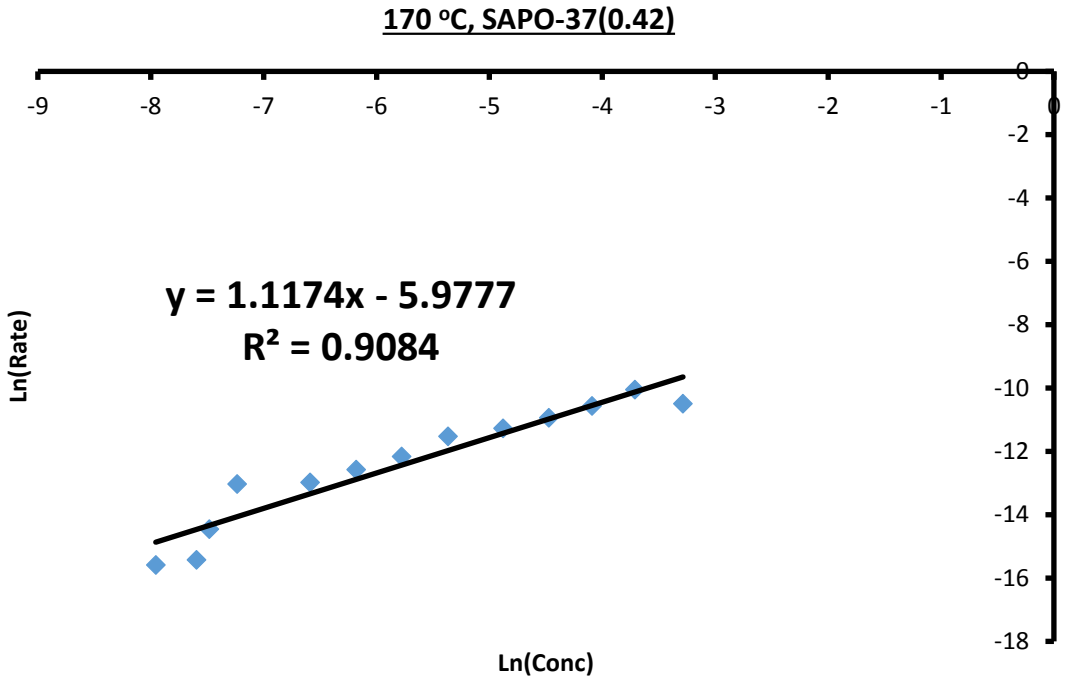

Figure S29: Graph detailing kinetic analysis of cyclohexanone oxime to ε-caprolactam with SAPO-37(0.42) at 170 °C

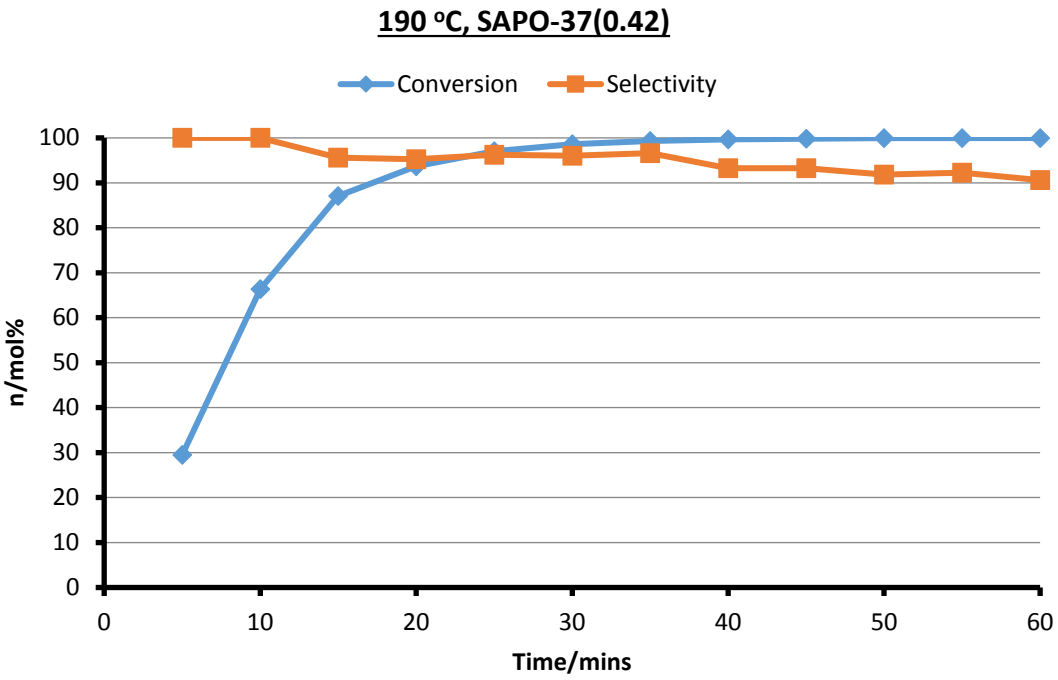

Figure S30: Catalytic data for the conversion of cyclohexanone oxime to ε-caprolactam with SAPO-37(0.42) at 190°C

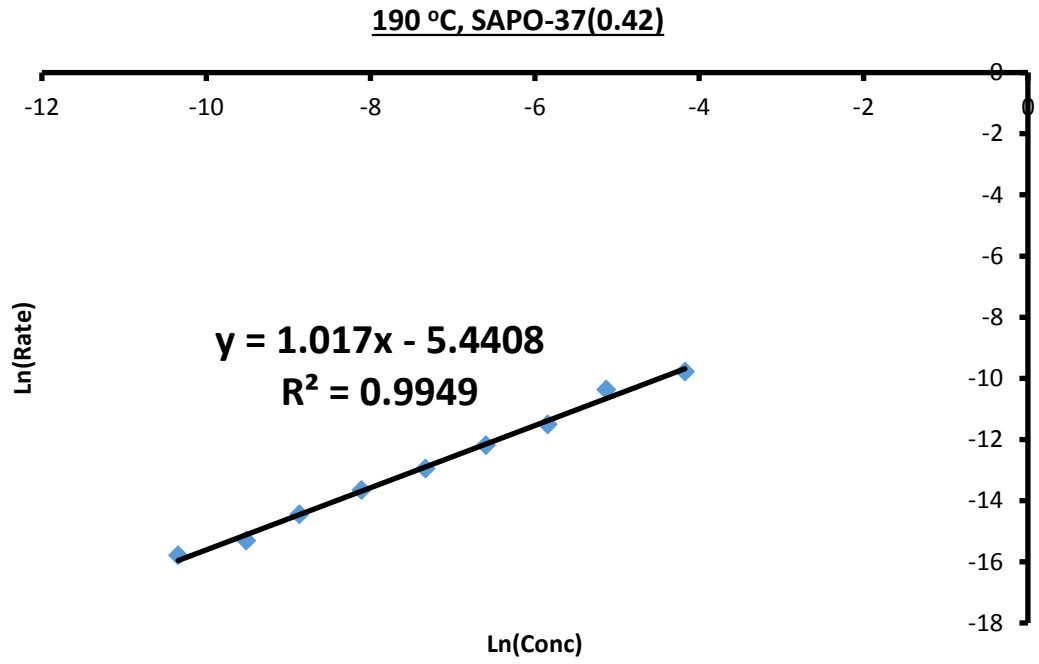

Figure S31: Graph detailing kinetic analysis of cyclohexanone oxime to ε-caprolactam with SAPO-37(0.42) at 190 °C

SAPO-37(0.63)

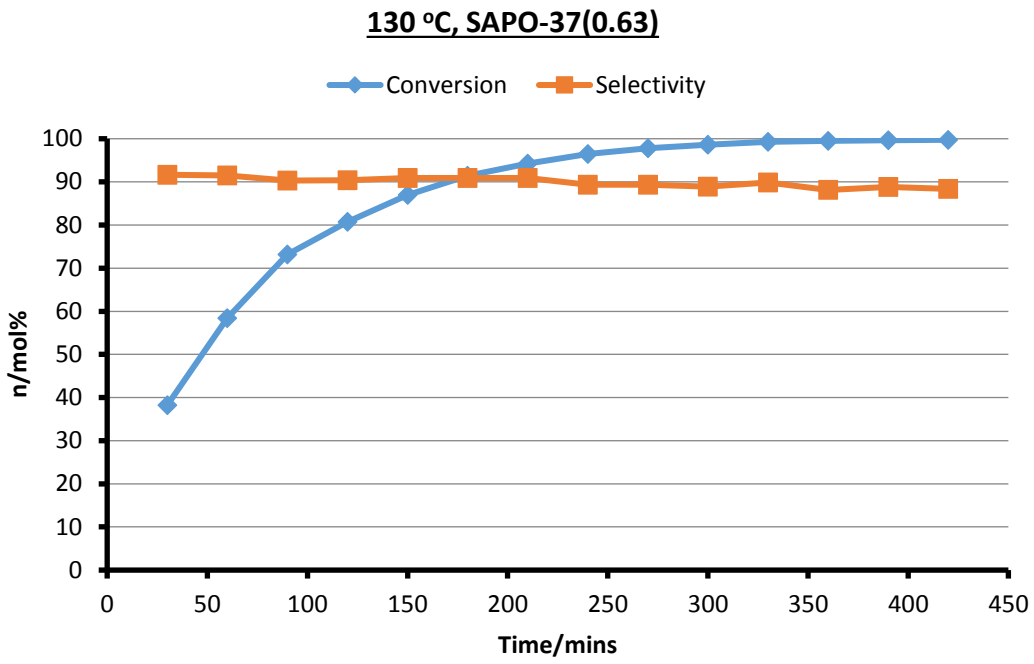

Figure S32: Catalytic data for the conversion of cyclohexanone oxime to ε-caprolactam with SAPO-37(0.63) at 130°C

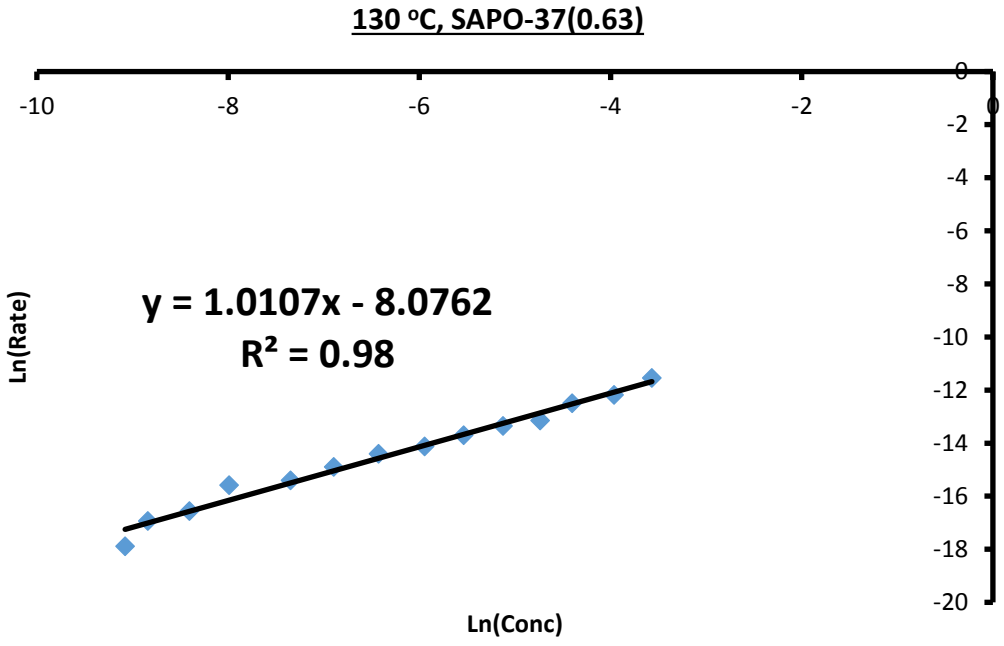

Figure S33: Graph detailing kinetic analysis of cyclohexanone oxime to ε-caprolactam with SAPO-37(0.63) at 130 °C

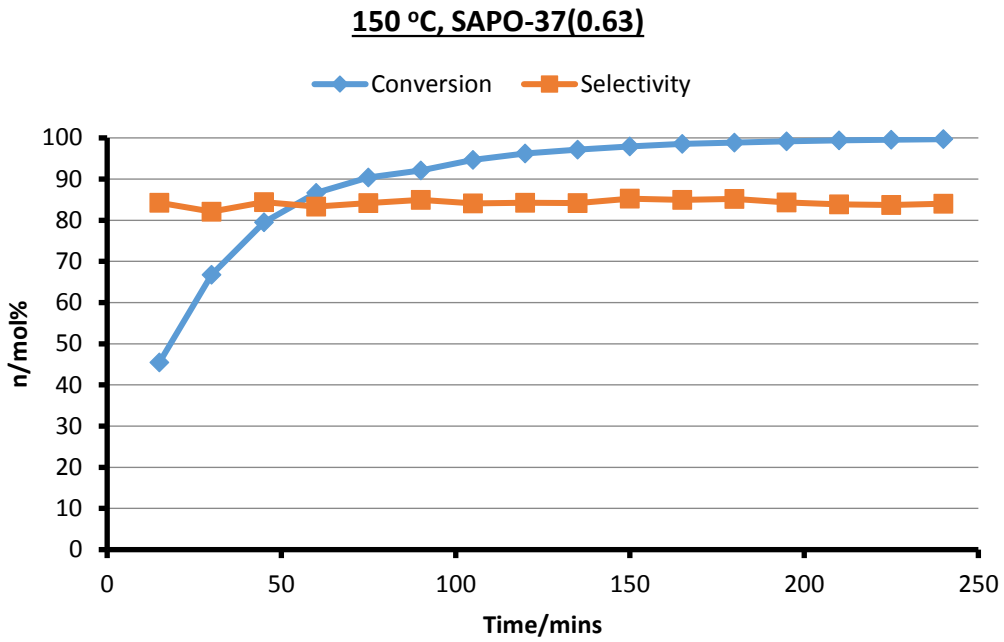

Figure S34: Catalytic data for the conversion of cyclohexanone oxime to ε-caprolactam with SAPO-37(0.63) at 150°C

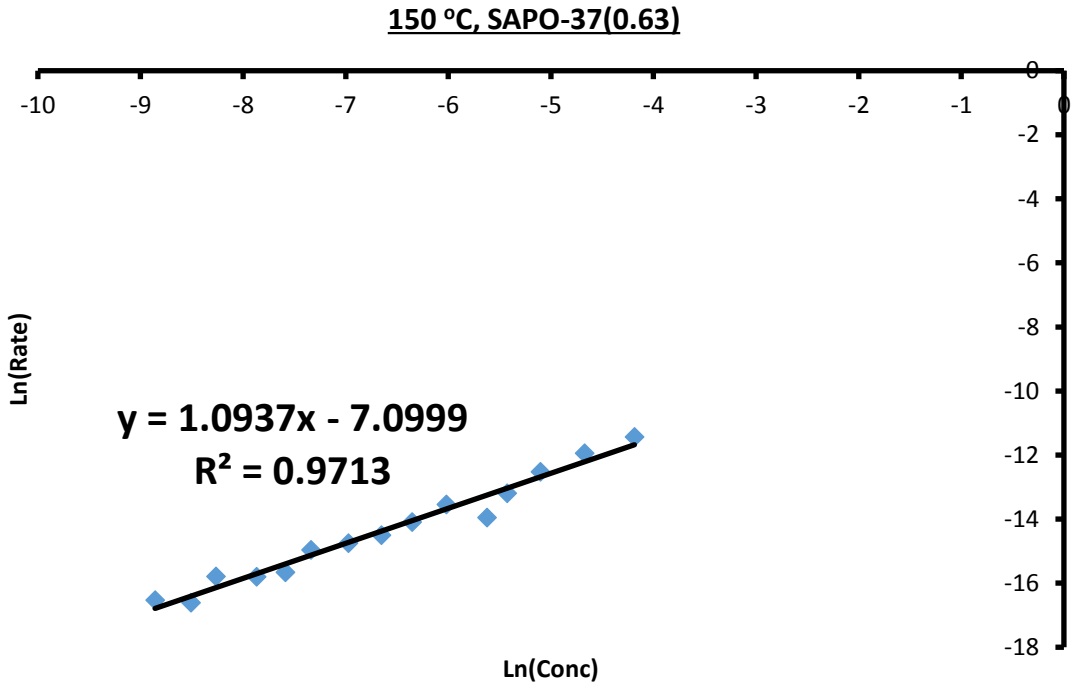

Figure S35: Graph detailing kinetic analysis of cyclohexanone oxime to ε-caprolactam with SAPO-37(0.63) at 150 °C

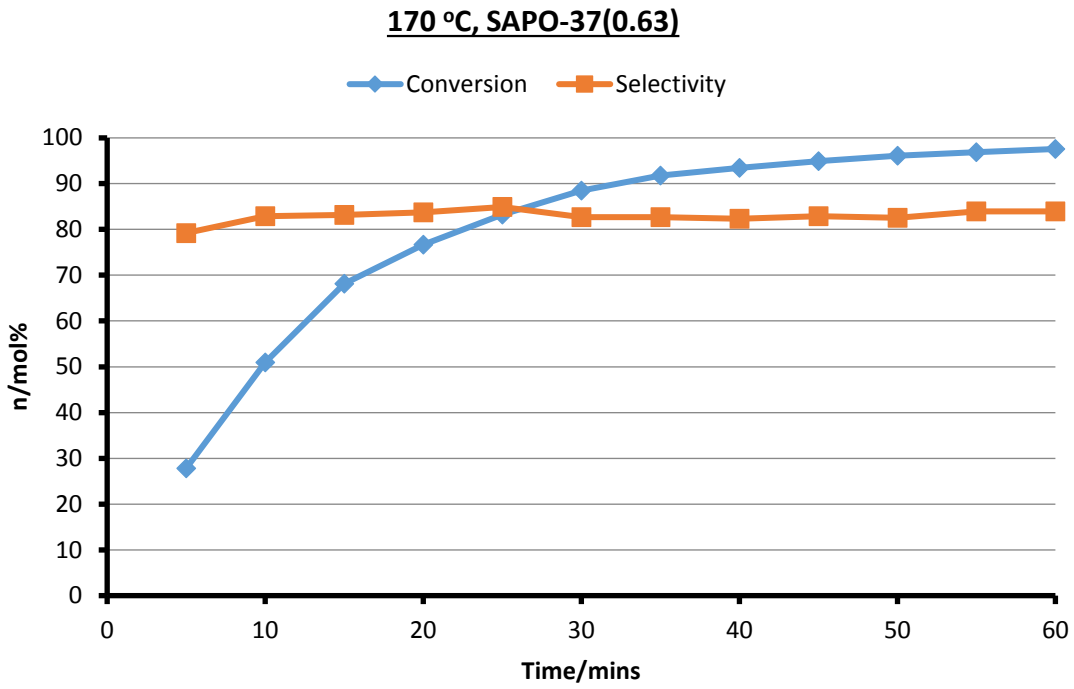

Figure S36: Catalytic data for the conversion of cyclohexanone oxime to ε-caprolactam with SAPO-37(0.63) at 170°C

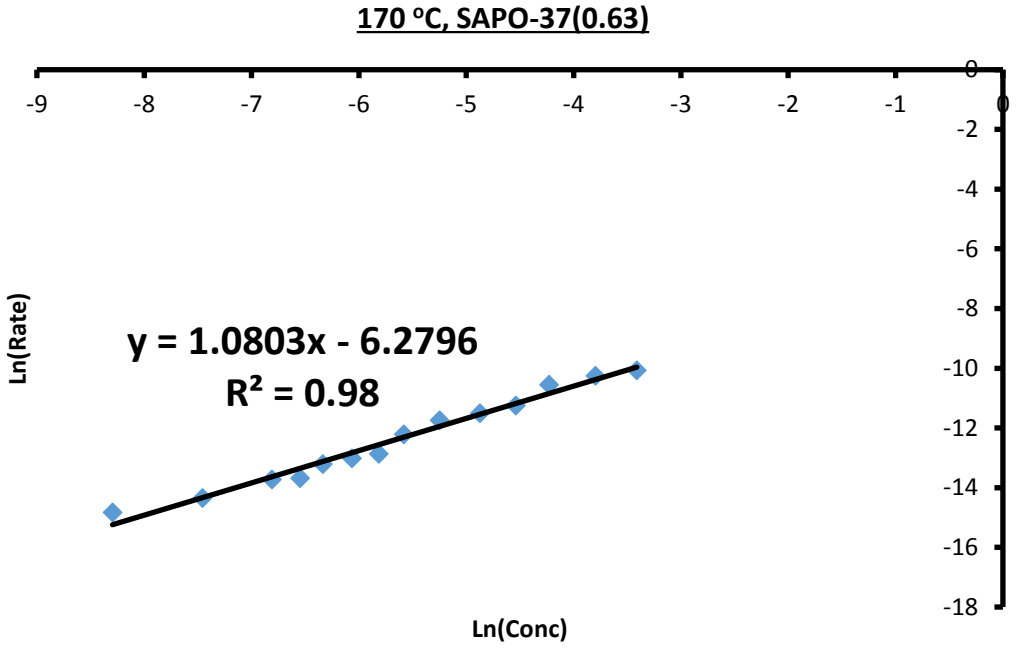

Figure S37: Graph detailing kinetic analysis of cyclohexanone oxime to ε-caprolactam with SAPO-37(0.63) at 170 °C

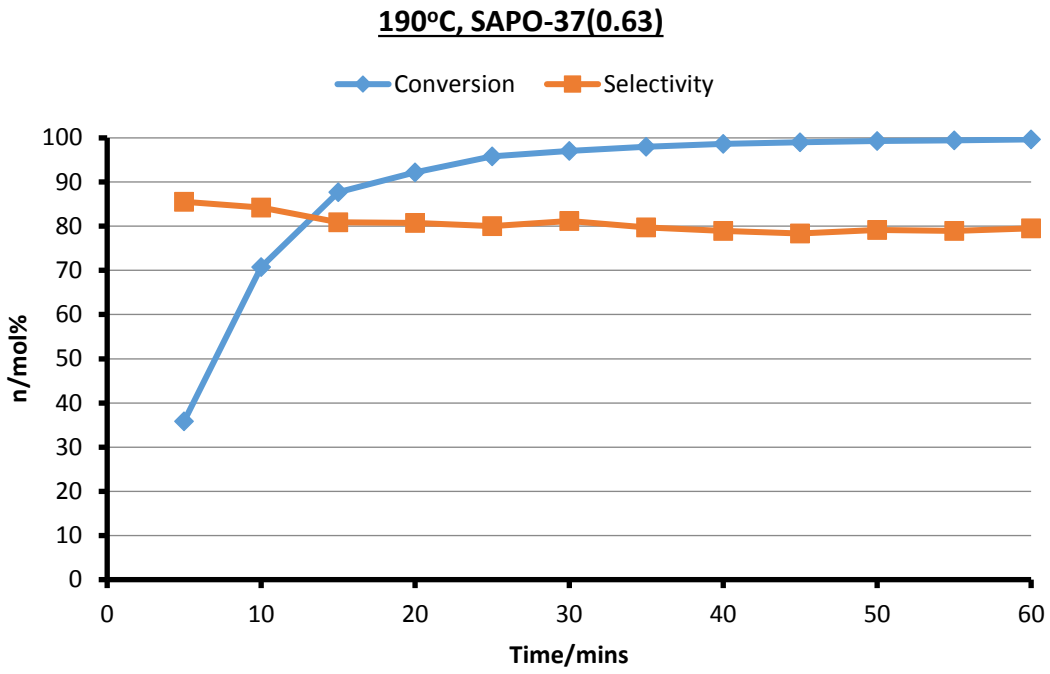

Figure S38: Catalytic data for the conversion of cyclohexanone oxime to ε-caprolactam with SAPO-37(0.63) at 190ºC

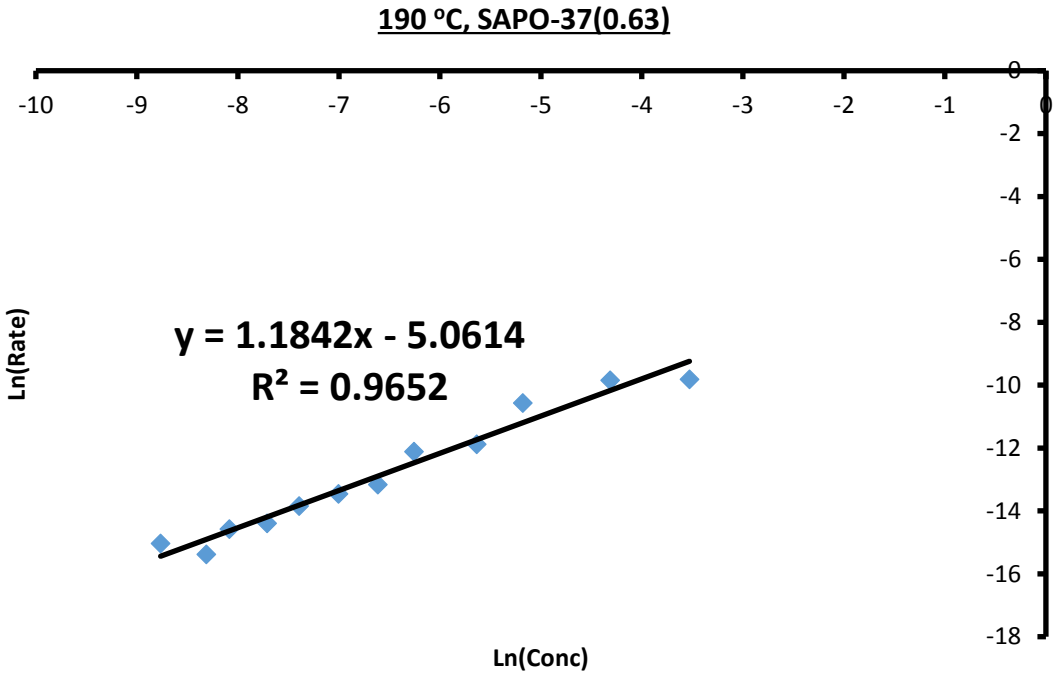

Figure S39: Graph detailing kinetic analysis of cyclohexanone oxime to ε-caprolactam with SAPO-37(0.63) at 190 ºC

Catalysis summary

Table S7: Summary of catalytic results for the low-temperature Beckmann rearrangement of cyclohexanone oxime to ε-caprolactam

Temperature/^{o}C	System	Time/mins	Conversion/mol%	ε-caprolactam selectivity/mol%[a]
130	SAPO-37(0.21)	180	89.3	96.0
		420	98.9	93.5
	SAPO-37(0.42)	180	89.8	93.3
		420	98.8	90.3
	SAPO-37(0.63)	180	90.4	90.9
		420	99.8	88.4
150	SAPO-37(0.21)	90	98.7	93.7
		240	100.0	90.8
	SAPO-37(0.42)	90	95.2	91.1
		240	99.9	88.7
	SAPO-37(0.63)	90	92.1	85.0
		240	99.7	84.1
170	SAPO-37(0.21)	40	98.6	90.4
		60	99.8	90.1
	SAPO-37(0.42)	40	95.5	88.8
		60	98.9	89.9
	SAPO-37(0.63)	40	93.5	82.3
		60	97.6	83.9
190	SAPO-37(0.21)	40	99.5	90.1
		60	99.9	89.8
	SAPO-37(0.42)	40	99.7	86.2
		60	100.0	85.4
	SAPO-37(0.63)	40	98.7	78.9
		60	99.7	79.5

Conditions: Catalyst:Cyclohexanone oxime:Benzonitrile ratio 1:1:200, 0.1 g of cyclohexanone oxime. a) Other products include cyclohexanone and products arising from solvent-oxime interactions.

Kinetic analysis

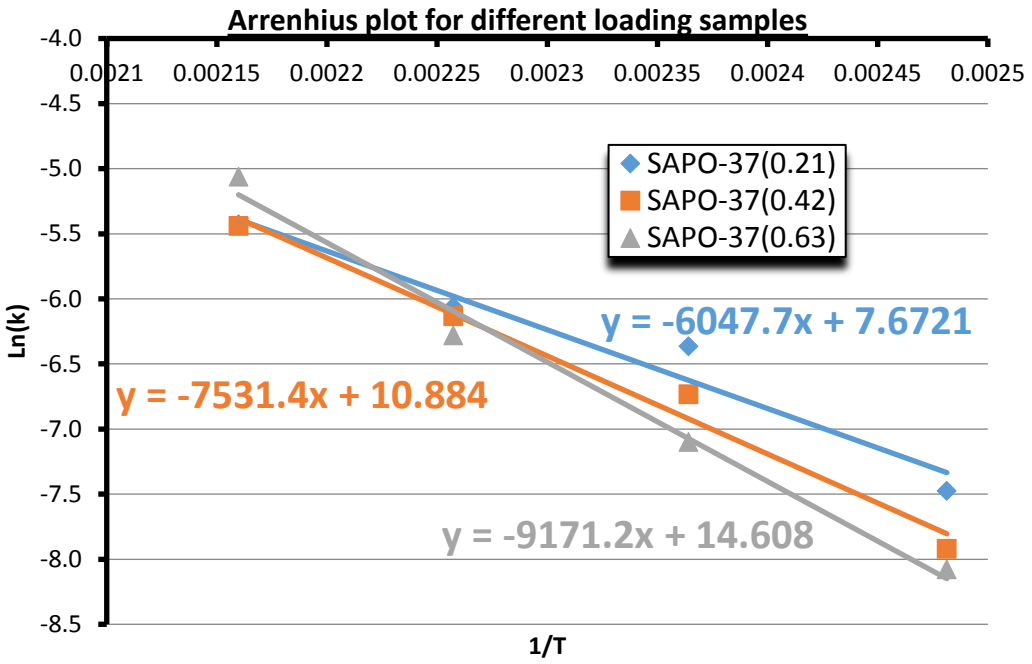

Figure S40: Arrenhius plot giving information on the activation energies of various SAPO-37 samples.

Table S8: Calculating of activation energy from the gradients obtained in Figure S46.

Sample	**$-E_a/R$**	**E_a/ kJ mol^{-1}**	**E_a/ kCal**
SAPO-37(0.21)	-6047.7	50.3	12.0
SAPO-37(0.42)	-7531.4	62.6	15.0
SAPO-37(0.63)	-9171.2	76.2	18.2

Anhydrous catalytic data

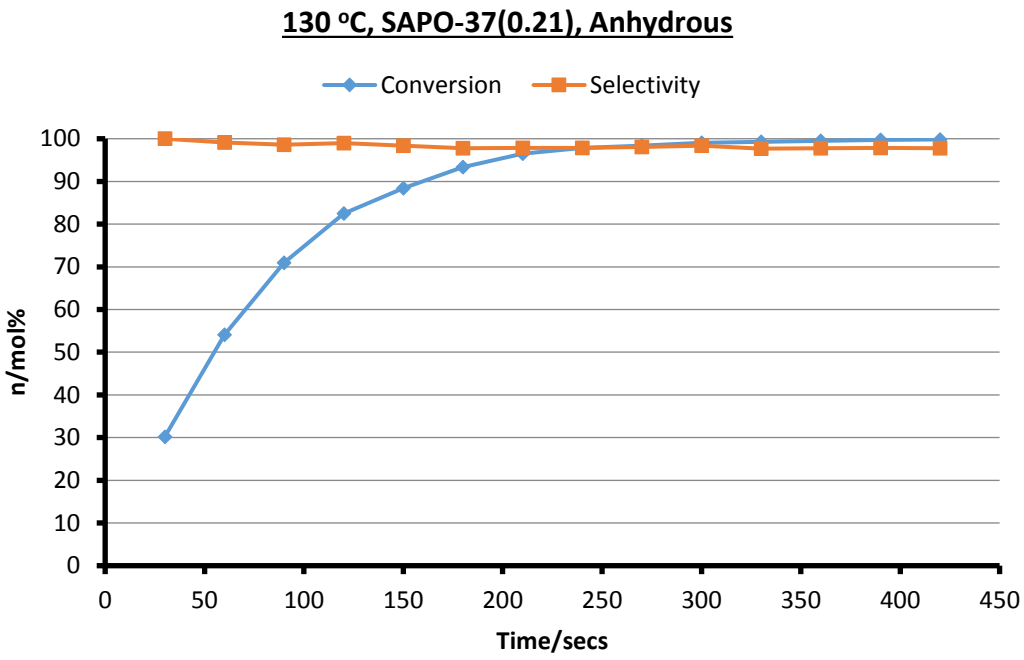

Figure S41: Catalytic data for the conversion of cyclohexanone oxime to ε-caprolactam with SAPO-37(0.21) at 130°C under anhydrous conditions

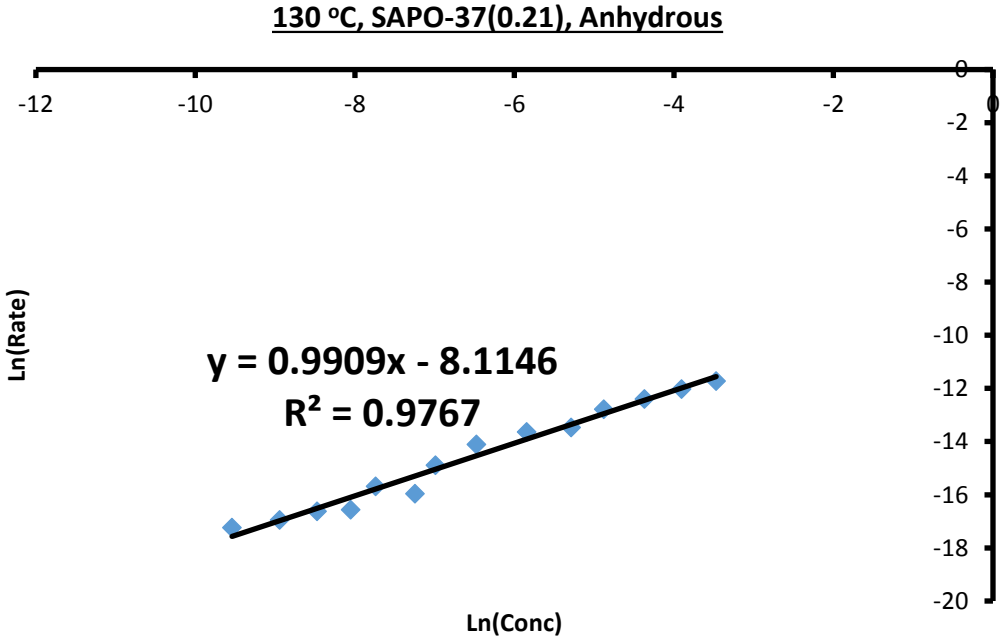

Figure S42: Graph detailing kinetic analysis of cyclohexanone oxime to ε-caprolactam with SAPO-37(0.21) at 130 °C under anhydrous conditions

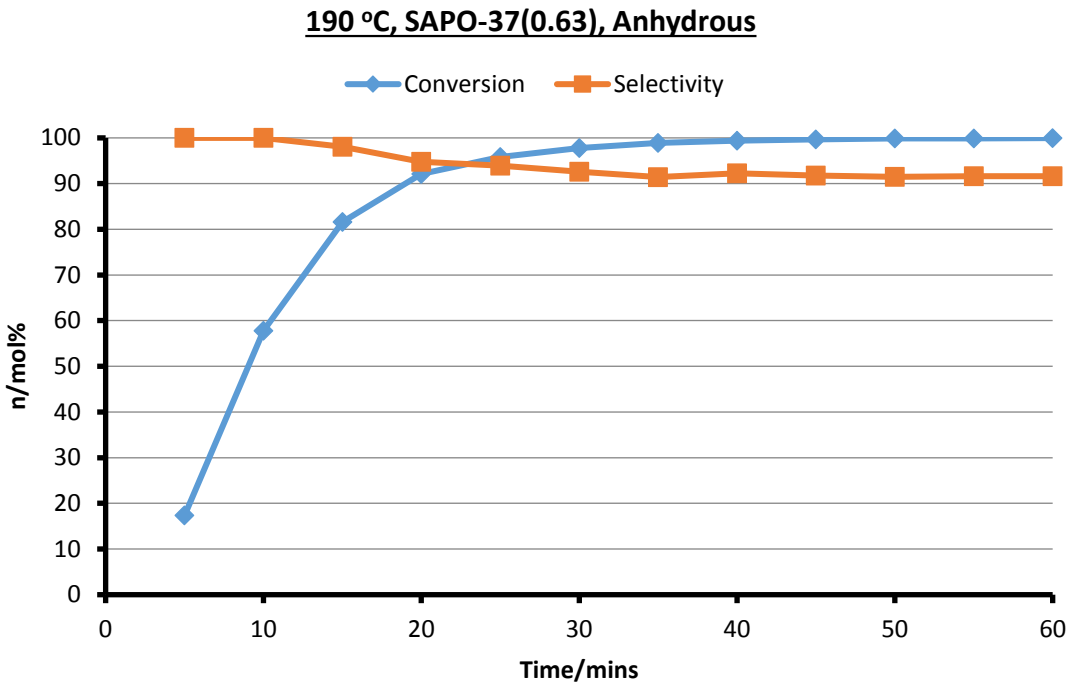

Figure S43: Catalytic data for the conversion of cyclohexanone oxime to ε-caprolactam with SAPO-37(0.63) at 190ºC under anhydrous conditions

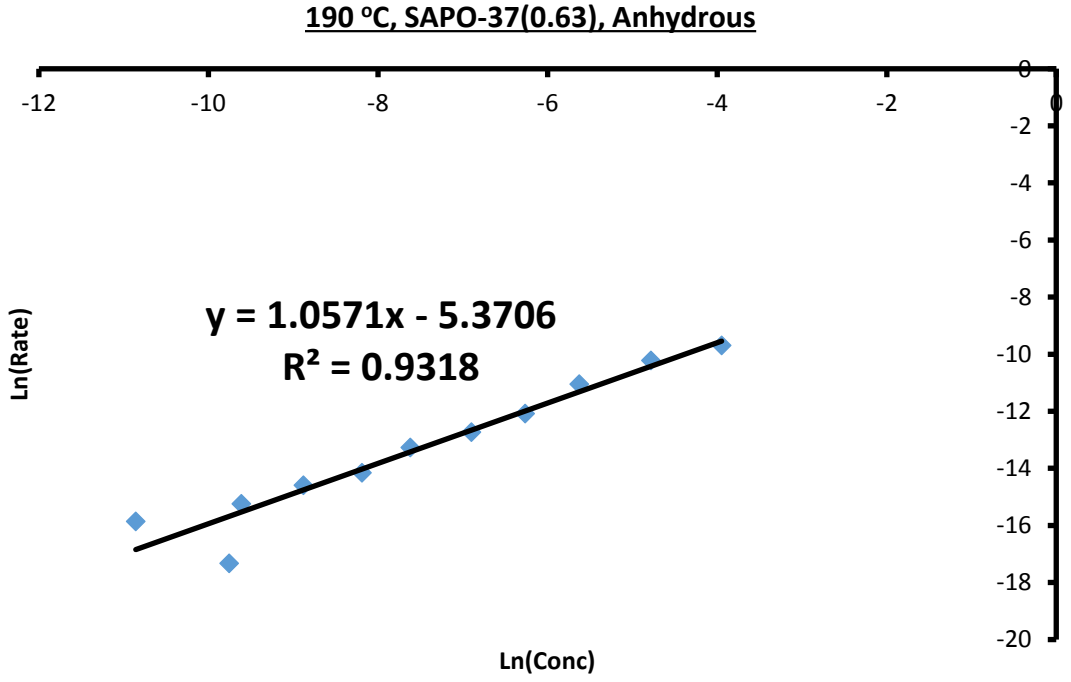

Figure S44: Graph detailing kinetic analysis of cyclohexanone oxime to ε-caprolactam with SAPO-37(0.63) at 190 ºC under anhydrous conditions

Table S9: Comparison of anhydrous and wet systems for the low temperature rearrangement of cyclohexanone oxime to ε-caprolactam

Temperature/°C	Sample	Time/mins	Conversion/mol%	ε-caprolactam selectivity/mol%[a]
130	SAPO-37(0.21) Anhydrous	120	82.5	99.0
		180	93.4	97.8
		420	99.8	97.8
	SAPO-37(0.21) Wet	120	78.1	96.1
		180	89.3	96.0
		420	98.9	93.5
190	SAPO-37(0.63) Anhydrous	20	92.1	94.7
		40	99.4	92.3
		60	99.9	91.6
	SAPO-37(0.63) Wet	20	92.2	80.8
		40	98.7	78.9
		60	99.7	79.5

Conditions: Catalyst:Cyclohexanone oxime:Benzonitrile ratio 1:1:200, 0.1 g of cyclohexanone oxime. a) Other products include cyclohexanone and products arising from solvent-oxime interactions.

Recycle data

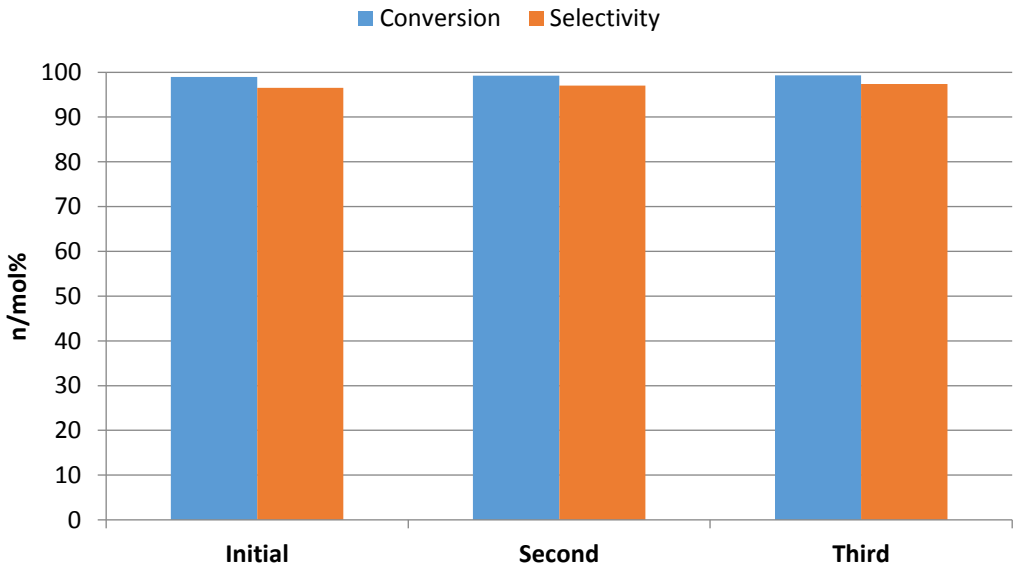

Figure S45: Plot detailing the recyclability of the SAPO-37(0.21) for the conversion of cyclohexanone oxime to ε-caprolactam at 130 °C under anhydrous conditions after reactivation cycles.

Proposed mechanism

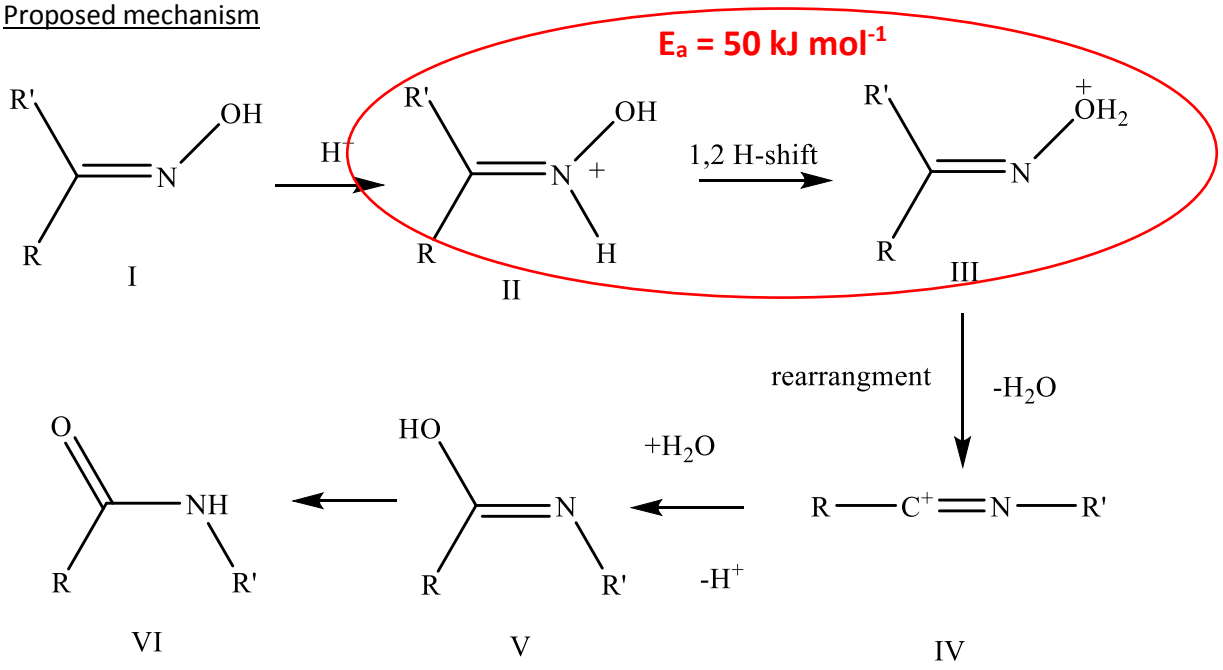

Scheme S4: Proposed mechanism for the liquid-phase Beckmann rearrangement.

Mass balance calculations

0.986 mmols of Chlorobenzene and 0.900 mmols of Cyclohexanone oxime were used in this reaction after 420 minutes at 130 °C the following values were found:

GC Area of Internal standard (Chlorobenzene - CB): 69017.71

GC Area of reactant (Cyclohexanone oxime - OX): 614.09

GC Area of product (ε-caprolactam - CPR): 43746.73

GC Area of by-product (BP): 637.02

Calibration of Chlorobenzene v Cyclohexanone oxime was found to be:

Moles(OX) = Moles(CB) x 1.2972 x Area(OX)/Area(CB)

Moles(OX) = 0.986 mmols x 1.2972 x 614.09/69017.71 = 0.0114 mmols

Moles(CPR) = Moles(CB) x 1.4516 x Area(CPR)/Area(CB)

Moles(CPR) = 0.986 mmols x 1.4516 x 43746.73/69017.71 = 0.9073 mmols

Moles(BP) = Moles(CB) x 1.0000 x Area(BP)/Area(CB)

Moles(BP) = 0.986 mmols x 1.0000 x 637.02/69017.71 = 0.0091 mmols

Total moles accounted for: 0.0114 + 0.9073 + 0.0091 = 0.9278 mmols = 103% mass balance

This also accounts for a conversion of 98.7% and a selectivity of 99.0%. This is within GC error.

Experimental

Catalysis synthesis

The standard synthesis procedure for SAPO-37 is outlined below and is typical for all samples examined in this study as per ref 1. Table S10 shows the variation in gel composition for the 4 different samples. Pseudo-boehmite was slowly added to a diluted solution of phosphoric acid (85 wt%) and left to stir for 7 hours. A second solution of tetramethylammonium hydroxide pentahydrate dissolved in tetrapropylammonium hydroxide (40 wt%) was prepared to which fumed silica was slowly added. This was left to stir for 2 hours and was then added dropwise to the stirred Al/P gel. The mixture stirred for 68 hours and was then transferred to an autoclave. The solution was heated under autogeneous pressure at 200^{o}C for 24 hours. On removal the gel was centrifuged, filtered and washed. The material was then dried overnight at room temperature. The white solid was then calcined at 550^{o}C for 16 hours and kept in an inert atmosphere.

Table S10: Gel loadings for SAPO-37 materials

Sample	Gel composition	Silicon content/wt%	BET/ m^2/g	Fd3m unit cell parameter/Å
SAPO-37(0.11)	$1.00H_3PO_4:0.67Al_2O_3:0.97TPAOH:0.025TMAOH:$**$\underline{0.11SiO_2}$**	N/A	N/A	N/A
SAPO-37(0.21)	$1.00H_3PO_4:0.67Al_2O_3:0.97TPAOH:0.025TMAOH:$**$\underline{0.21SiO_2}$**	3.0	588	24.31
SAPO-37(0.42)	$1.00H_3PO_4:0.67Al_2O_3:0.97TPAOH:0.025TMAOH:$**$\underline{0.42SiO_2}$**	7.6	601	24.58
SAPO-37(0.63)	$1.00H_3PO_4:0.67Al_2O_3:0.97TPAOH:0.025TMAOH:$**$\underline{0.63SiO_2}$**	9.5	563	24.64

SAPO-5, -34 and -41 were prepared as per references 2 and 3.

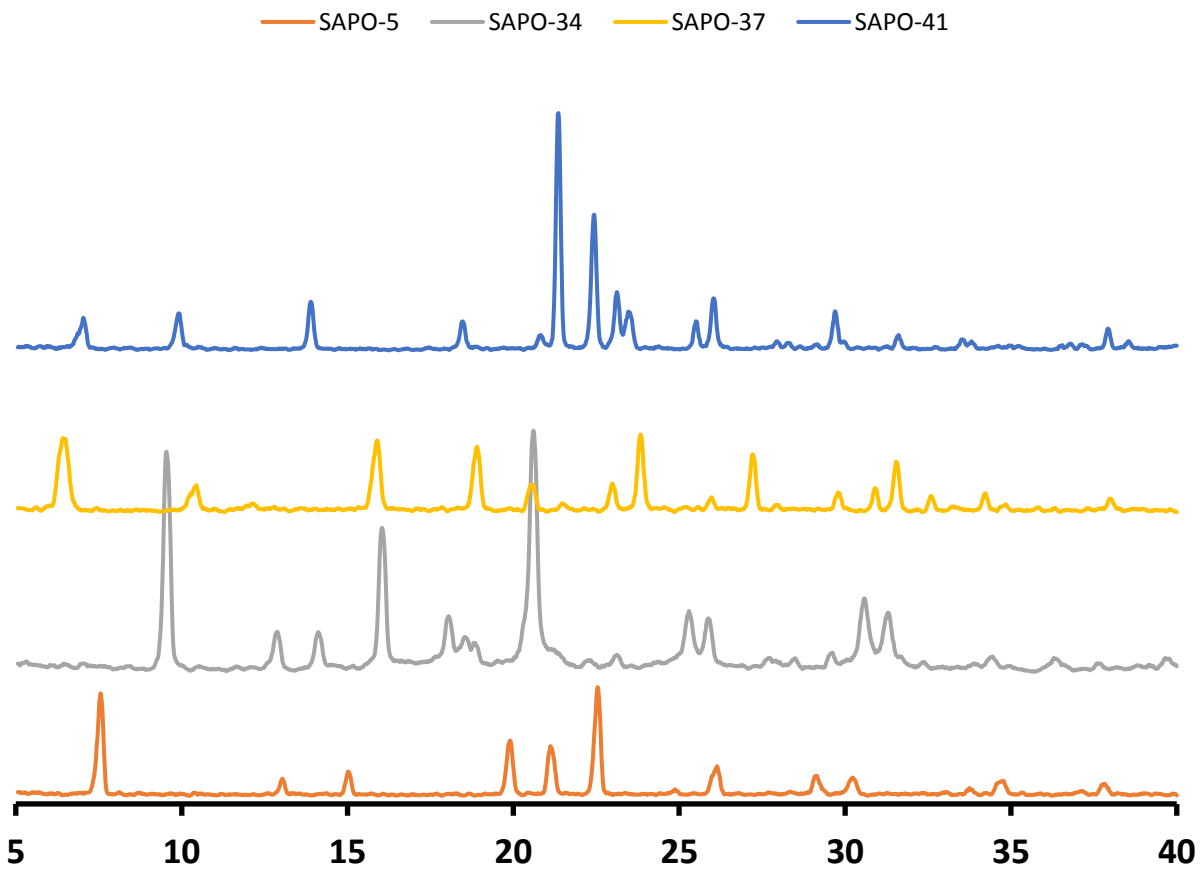

Figure S46: Powder XRD patterns of the calcined SAPOs, confirming their phase purity.

Inelastic neutron scattering spectroscopy

The SAPO-37 was dried under a flow of He gas at 550 °C for 2 hours.

A 1:10 solid-state mixture of cyclohexanone oxime and SAPO-7 was prepared in a glove box, under argon atmosphere. The mixture was transferred to an aluminium-foil sachet, which was loaded into an indium wire-sealed aluminium can in the glovebox.

The experiments were carried out using high-flux INS spectrometer MAPS at the ISIS Pulsed Neutron and Muon Source, (Oxfordshire, UK). The cans were placed in a top-loading closed cycle refrigerator cryostat in order to take low-temperature readings (< 10 K). Measurements were taken at neutron incident energies of 650 meV ('A' chopper speed 600 Hz), 250 meV ('A' chopper speed 400 Hz) and 100 meV ('A' chopper speed 200 Hz). The samples were heated to the temperatures noted in figure 2, and then sequentially cooled to <30 K for the INS measurement between each heating step. The same procedure was employed for the pure compounds of cyclohexanone oxime and ϵ-caprolactam.

ICP analysis

A Perkin-Elmer Optimum 3000 DV was used for ICP analyses with calcined samples prepared and fully digested in 10ml of deionised water and 10ml of ACS Plus Certified H_2SO_4 (Fisher Scientific). Solutions of standard concentrations were used for calibration.

BET surface area measurements

BET surface area measurements were performed using a Micromeritics Gemini 2375 surface area analyser and prepared using flow gas preparation.

Scanning electron microscopy

Scanning electron microscopy images were obtained using a JOEL-JSM5910 microscope with accelerating voltage of 0.3-30 kV. The samples were prepared by carbon coating.

Powder X-ray diffraction

Powder X-Ray diffraction patterns were obtained using a Siemens D5000 diffractometer using Cu $K_{\alpha 1}$ radiation, whereby λ = 1.54056 Å.

NMR measurements

All NMR measurements were performed on a Chemagnetics Infinity 400 spectrometer on a 4mm MAS double-resonance probe. For all samples, approximately 100 mg of material was quickly transferred in a thin wall zirconium oxide rotor and then spun at 8kHz using compressed nitrogen, in order to prevent sample degradation in air, for bearing, drive and purge. The nitrogen gas was generated in-house from evaporation of liquid nitrogen in high pressure 1300 litre tanks suitably connected to the NMR facility. ^{27}Al NMR experiments were performed using direct acquisition (128 scans with and a pulse delay of 2s between scans). ^{31}P NMR data were acquired both with direct acquisition (4 scans and 120s delay between scans) and with ramped cross-polarization[4] (2s delay between scans), but only the direct acquisition data are shown in Fig.S18. ^{29}Si NMR data for all 1D experiments were performed using cross-polarization and SPINAL64 decoupling.[5] Typical spectra were acquired with 8192 scans and 2s between scans. Two dimensional experiments were performed using proton-driven spin diffusion (PDSD)[6] with a mixing time of 5ms and 160 t_1 increments of 62.5μs, for a total acquisition time of 23 hours. Phase sensitive spectra were obtained using the TPPI approach. The chemical shift axes in the ^{27}Al, ^{31}P and ^{29}Si spectra were referenced using 1M $AlCl_3$ aqueous solution (0ppm), 85% H_3PO_4 (0ppm) and silicon rubber

(–22.42ppm) respectively, following the convention described in ref 7. The NMR data was processed using matNMR.[8]

Temperature-programmed-desorption

All TPD measurements were performed on a custom built system using TCD detectors to monitor ammonia concentration. As-synthesised materials were pretreated by heating at 10°C/min to 550ºC in a 20% O_2/ helium mixture [Matheson UHP grade passed through a Drierite/molecular sieve gas purifier (Alltech Associates)] and held for 2 hours. The samples were exposed to ammonia and allowed to equilibrate at 150ºC for 8 hours. Desorption was performed in flowing helium[Matheson UHP grade further purified with an Oxy-Trap (Alltech Associates) and an indicating OMI-1 purifier (Supelco)] at 10°C/min to 600°C and held for 40 minutes at 600ºC.

Low temperature CO adsorption FT-IR

All IR experiments were performed in a custom designed IR flow cell that allowed for sample heating and cryogenic cooling. As-synthesised samples were ground and pressed into 13mm diameter self-supporting pellets (~8 mg/cm^2) and heated at 10 °C/min to 550 °C in a mixture of 20 % O_2 in N_2 [Matheson UHP grade further purified using a P400 air purifier(VICI)] and held for 1 hour. The flow was then switched to helium[Matheson UHP grade further purified using a P-100 helium purifier(VICI) and an indicating OMI-1 purifier(Supelco)] and held for an additional hour. The system was then cooled to ~-175°C and a spectrum recorded. Nine 0.02 cm^3 injections of CO (Matheson research purity) were added to the system followed by a final injection of 0.20 cm^3. After each injection, the system was equilibrated for 3 minutes and a spectrum recorded. All spectra were collected on a Nicolet Nexus 870 FTIR spectrometer using a cooled MCT detector. Each spectrum was obtained by co-adding 128 scans at a resolution of 2 cm^{-1}. All spectral processing was done using the GRAMS/AI 9 software (Thermo Scientific). All spectra are normalized to a 10 mg pellet weight. Difference spectra were obtained by subtracting the spectrum of the sample before adsorption of the probe molecule.

Collidine adsorption FT-IR

As-synthesised samples were ground and pressed into 13mm diameter self-supporting pellets (~8 mg/cm^2) and heated at 10 °C/min to 550 °C in a mixture of 20 % O_2 in N_2[Matheson UHP grade further purified using a P400 air purifier(VICI)] and held for 2 hours. The system was then cooled to 30 °C and a spectrum recorded. The sample was equilibrated with collidine (helium saturated with collidine vapor at 7ºC) for 1 hour at 150ºC. Stepwise desorption of collidine was done at 150, 300 and 450°C. After an hour hold at desorption temperature, the sample was cooled to room temperature and a spectrum recorded. All spectra were collected on a Nicolet Nexus 870 FTIR spectrometer using a cooled MCT detector. Each spectrum was obtained by co-adding 128 scans at a resolution of 2 cm^{-1}. All spectral

processing was performed using the GRAMS/AI 9 software (Thermo Scientific). All spectra were normalized to a 10 mg pellet weight. Difference spectra were obtained by subtracting the spectrum of the sample before adsorption of the probe molecule.

Catalysis reaction

100 mg of cyclohexanone oxime, 100 mg of catalyst and 20ml of benzonitrile (Aldrich) were but into a glass reactor and stirred at 500 rpm at the appropriate temperature (130, 150, 170 and 190 ^{o}C) under reflux. Samples were taken at appropriate intervals (30, 15, 5 and 5 minutes respectively).

For anhydrous conditions a nitrogen bubbler was attached to the top of the condenser. A glass reactor containing cyclohexanone oxime and the catalyst was purged with nitrogen for five minutes before 20 ml of anhydrous benzonitrile (Aldrich) was injected through into the vessel using a dry needle and syringe. The system was then lowered into the pre-heated oil-bath and stirred at 500 rpm under a steady flow of nitrogen. Samples were taken at appropriate intervals (30 minutes for 130 ^{o}C, 5 minutes for 190 ^{o}C) via a clean, dry needle and syringe. Samples were analysed as above.

All samples were analysed on a Varian Star 3400CX gas chromatogram with flame ionization detector (FID). Samples were injected into a Perkin Elmer a HP1 cross linked methylsiloxane (30 m x 0.32 mm x 1 µm film thickness) column. The samples were mass balanced using chlorobenzene as an internal standard. The following GC method was used:

Start at 120^{o}C, Hold 2 minutes, Ramp at 15^{o}C/min up to 220^{o}C, Hold for 5 minutes at 220^{o}C. The method is 13 minutes and 40 seconds long in total. The benzonitrile solvent peak is a large peak at 3.5 minutes, the cyclohexanone oxime is at 4.0 minutes, ε-caprolactam peak is at 5.8 minutes, the by product is at 6.6 minutes.

The injector port is set to 220^{o}C, the detector is set to 250^{o}C. The carrier pressure (Helium) is at 14 psig. The method is given 1 minute to equilibrate before injection. Typically 5µl of centrifuged sample is injected.

The samples were calibrated using a relative response factor of ε-caprolactam relative to cyclohexanone oxime, this was found to be 1.119. The samples were calibrated to an internal standard of chlorobenzene for the mass balance. Cyclohexnaone oxime was fousdn to have a relative response factor of 1.2972 relative to chlorobenzene, and ε-caprolactam was found to have a response factor of 1.4516, the mass balance at 130^{o}C was found to be 106% after 6 hours.

The response factors were used to calculate the moles of cyclohexanone oxime, ε-caprolactam and by-products (response factor assumed to be 1.00). The conversion is calculated as:

Conversion = 100x(initial moles of oxime – moles of oxime detected)/initial moles of oxime

Selectivity = 100x(moles of caprolactam)/moles of products detected

Kinetics and derivations

The rate of the reaction at time t was calculated by comparing the concentrations and times with that of the previous sample thus:

$$Rate_t = ([Cyclohexanone\ oxime]_t - [Cyclohexanone\ oxime]_{t-1})/(Time_t - Time_{t-1})$$

The order and rate constant of the reaction were then found through manipulation of the equation below:

$$Rate = k[Cyclohexanone\ oxime]^n$$

where k is the rate constant and n is the order of the reaction:

$$Ln|Rate| = Ln|k[Cyclohexanone\ oxime]^n]|$$

$$Ln|Rate| = Ln|k| + Ln|[Cyclohexanone\ oxime]^n|$$

$$Ln|Rate| = Ln|k| + nLn|[Cyclohexanone\ oxime]|$$

$$y = Ln|k| + n.x$$

By plotting Ln|Rate| v Ln|[Cyclohexanone oxime]| the Ln|k| and the order of the reaction are shown as the y-intercept and gradient respectively.

The activation energies were calculated through manipulation of the Arrenhius equation:

$$k = A.exp(-E_a/RT)$$

where k is the rate constant, A is the pre-exponential factor, E_a is the activation energy in kJ mol^{-1}, R is the perfect gas constant (8.314 J K^{-1} mol^{-1}) and T is the temperature in Kelvin.

$$Ln|k| = Ln|A.exp(-E_a/RT)|$$

$$Ln|k| = Ln|A| + Ln|exp(-E_a/RT)|$$

$$Ln|k| = Ln|A| - E_a/RT$$

$$y = Ln|A| + (-E_a/R)x$$

By plotting Ln|k| against 1/T the activation energy is found by multiplying the gradient by -8.314 J K^{-} mol^{-1}.

Recycles

After a reaction the catalyst was collected via filtration, washed with fresh benzonitrile (~20 ml) and distilled water (~50 ml) and dried at 80 ^{o}C overnight. The material was then reactivated through calcination and re run as above.

References

1. Jappar, N.; Tanaka, Y.; Nakata, S.; Tatsumi, T. *Micro. Meso. Mater.*, **1998**, 23, 169-178
2. P. Meriaudeau, V. A. Taun, V. T. Ngheim, S. Y. Lai, L. N. Hung and C. Naccache, *J. Catal.*, **1997**, 169, 55-66.
3. Potter, M.E.; Cholerton, M. E.; Kezina, J.; Bounds, R.; Carravetta, M.; Manzoli, M.; Gianotti, E.; Lefenfeld, M.; Raja. R. *ACS Catal.* **2014**, 4, 4161-4169.
4. Metz, G.; Wu, X.; Smith, S.O. *J. Magn. Reson. A*, **1994**, 110, 219-227
5. Fung, B.M.; Khitrin, A.K.; Ermolaev, K. *J. Magn. Reson. A*, **2000**, 142, 97-101
6. Szeverenyi, N. M.; Sullivan, M. J.; Maciel, G. E. *J. Magn. Reson.* **1982**, 47, 462-475
7. Hayashi, S.; Hayamizu K. *Bull. Chem. Soc. Jpn,* **1989**, 62, 2429-2430
8. van Beek, J.D. *J. Magn. Reson.*, **2007**, 187, 19-26